Title

Progress in Understanding Short-Range Structure in Nuclei: An Experimental Perspective

Authors

Arrington, John

Fomin, Nadia

Schmidt, Axel

Publication Date

2022-09-26

DOI

10.1146/annurev-nucl-102020-022253

ANNUAL REVIEWS

Annual Review of Nuclear and Particle Science

Progress in Understanding Short-Range Structure in Nuclei: An Experimental Perspective

John Arrington,[1] Nadia Fomin,[2] and Axel Schmidt[3]

[1]Lawrence Berkeley National Laboratory, Berkeley, California, USA; email: jarrington@lbl.gov

[2]Department of Physics and Astronomy, University of Tennessee, Knoxville, Tennessee, USA

[3]Department of Physics, The George Washington University, Washington, DC, USA

Annu. Rev. Nucl. Part. Sci. 2022. 72:307–37

The *Annual Review of Nuclear and Particle Science* is online at nucl.annualreviews.org

https://doi.org/10.1146/annurev-nucl-102020-022253

Keywords

high-energy electron–nucleus scattering, short-range nucleon–nucleon correlations, deep inelastic electron scattering, nuclear structure functions, superfast quarks

Abstract

High-energy electron scattering is a clean, precise probe for measurements of hadronic and nuclear structure and plays a key role in understanding the role of high-momentum nucleons (and quarks) in nuclei. Jefferson Lab has dramatically expanded our knowledge of the high-momentum nucleons generated by short-range correlations, providing sufficient insight to model much of their impact on nuclear structure in neutron stars and in low- to medium-energy scattering observables, including neutrino oscillation measurements. These short-range correlations also seem related to the modification of the quark distributions in nuclei, and efforts to improve our understanding of the internal structure of these short-distance and high-momentum configurations in nuclei will provide important input on a wide range of high-energy observables.

Contents

1. INTRODUCTION

The structure of atomic nuclei is well described by mean-field calculations, which can reproduce a wide range of static properties and low-energy scattering observables over the full range of the periodic table. For some observables at higher energy scales, the contribution of nucleons with momenta above the Fermi momentum, k_F, becomes more important; it has been a long-time goal of higher-energy nuclear structure experiments to isolate and study these contributions. While the contribution from nucleons above k_F to the momentum distribution of nucleons in nuclei is low, the fact that they are at large momenta and (as discussed below) are associated with large excitation of the residual $(A-1)$ nucleus makes them an important piece of nuclear structure and gives them a dominant role in certain high-energy scattering observables.

These high-momentum nucleons are generated by the short-distance part of the nucleon–nucleon (*NN*) potential—the strong tensor attractive component for separations near 1 fm, and the repulsive core at shorter distances. Hard *NN* interactions at short distances generate pairs of nucleons with large relative momenta but small total momentum; these pairs are known as short-range correlations (SRCs). This leads to a picture of the nucleus where nucleons with momenta below k_F are dominated by the mean-field structure of complex many-body nuclei, while the structure at larger momenta is dominated by the two-body physics associated with the short-distance *NN* interaction.

Because of the underlying two-body physics, these contributions are similar in scattering from heavy nuclei or scattering from the deuteron. In principle, this makes it possible to combine

information from a variety of different observables in different nuclei to elucidate the nature of SRCs and to map out their strength and structure in light and heavy nuclei.

Electron scattering provides a clean and powerful probe of nuclear structure through the combination of the point-like nature of the probe, the well-understood interaction via virtual photon exchange, and the fact that the electromagnetic interaction allows a uniform probe of the entire nuclear volume. However, several complications arise when trying to isolate the high-momentum components of the nuclear wave function, and our understanding of the structure of SRCs comes from a combination of different measurements; each yields unique yet limited information, but together they provide an ever clearer picture of these important but poorly understood components of nuclear structure.

For the early theoretical foundations regarding SRCs, readers are referred to References 1 and 2. Additional examinations of the experimental considerations for probing SRCs are presented in References 3 and 4. More recent reviews include References 4–6, but significant experimental progress has been made since these works were published. In this review, we provide a brief overview of early studies and a more complete view of recent experimental progress and efforts to tie together information from different experiments. We also highlight key remaining questions and future experimental work.

2. MEASUREMENTS OF HIGH-MOMENTUM NUCLEONS AND SHORT-RANGE CORRELATIONS

One important consideration is that the momentum distribution of nucleons in a nucleus is not an experimental observable. Most experiments work in the framework of the plane-wave impulse approximation (PWIA), where the $A(e, e'p)$ cross section is connected to the spectral function, which accounts for both the momentum and energy distribution of the nucleons. In this case, the spectral function (or momentum distribution) is directly related to the cross section in the PWIA assumption, so direct comparison of the cross section with calculations based on a momentum distribution of the spectral function is possible. This is the approximation we make when we discuss the use of cross-section data to study the momentum distribution or the spectral function of nuclei.

We begin by highlighting early attempts to probe the distribution of nucleons at large momenta using $A(e, e'p)$ measurements, and we note some of the issues with interpreting these data. We then summarize how SRCs were isolated in inclusive scattering with a handful of precision measurements mapping out the relative contribution of SRCs in nuclei. Next, in Section 3, we discuss studies of the momentum distribution of SRCs in nuclei as well as their internal isospin and momentum structure.

2.1. Challenges in Isolating and Measuring High-Momentum Nucleons

In the PWIA, one can treat the $A(e, e'p)$ $1N$ knockout reaction as billiard-ball scattering from a single proton with $(A - 1)$ spectator nucleons. By knowing the electron beam energy and detecting the scattered electron and knocked-out proton, one has enough information to reconstruct the initial momentum and energy of the struck proton, which are referred to as the missing momentum (p_m) and missing energy (E_m). In principle, this should allow extraction of the proton distribution in the nucleus, but effects beyond the PWIA create significant challenges.

The potential for large contributions from meson-exchange currents (MECs) and final-state interactions (FSIs) makes probing the momentum distribution difficult, especially for large values of missing momentum and even for light nuclei (3, 4). Proton knockout measurements from the deuteron, conducted at Jefferson Lab over a wide kinematic range (7, 8), have been used to examine FSIs, and comparisons with the generalized Eikonal approximation (9) show that this

formalism provides a reasonable description of FSIs over a large kinematic range. However, recent measurements have pushed such studies to higher four-momentum transfer, Q^2, and larger p_m, focusing on regions of minimal FSIs, and none of the calculations reproduces the data above $p_m = 700$ MeV/c. Given this fact and the lack of high-precision systematic studies, it is not yet clear to what degree the FSI corrections can be minimized or corrected for. Therefore, SRC studies have generally moved away from $A(e, e'N)$ measurements except for comparisons of proton and neutron knockout, where these effects are assumed to have significant cancellation. These are described in more detail in Section 3.2.1, where we discuss progress in exclusive studies.

Inclusive scattering has also been used to study the momentum distribution of nucleons. The shape of the quasi-elastic (QE) peak is driven by the *e-p* and *e-n* elastic cross sections smeared by the nucleon momentum distributions (10), with scattering below the kinematic threshold for stationary nucleons, allowing for clean separation of QE from inelastic scattering. Under certain assumptions, y scaling (10–12) provides a connection between the QE cross section and the underlying momentum distribution. However, this relies on the PWIA, and MECs and FSIs can yield large corrections at low Q^2. It also assumes a final spectator $(A - 1)$ nucleus in an unexcited state, which is a poor approximation for scattering from an SRC within a nucleus. Model-dependent corrections [e.g., y_{CW} or y^* scaling (13, 14)] have been proposed to account for this limitation, but it is difficult to quantify the uncertainty in such an approach. We note, however, that in QE scattering from the deuteron at high Q^2, the y-scaling assumptions appear to be reasonable, and momentum distributions extracted from such data are in good agreement with momentum distributions calculated from realistic *NN* potentials, as shown in Reference 15.

2.2. Experimental Signatures of Short-Range Correlations

As noted in the previous section, the shape of the QE peak is driven by the distribution of protons and neutrons in the nucleus. One can decompose the cross section into contributions based on the structure (in particular high-momentum nucleons) in the breakup of the nucleus. In the naive SRC model (16), the cross section is separated into scattering from single nucleons in the nucleus with the spectator in an unexcited or minimally excited state, scattering from 2*N* SRCs where the final state is dominated by the high-momentum spectator and an $(A - 2)$ residual nucleus, and contributions from multinucleon SRCs where multiple nucleons in the initial state have large momenta. The bulk of the cross section comes from the first term, which represents the shell structure of the nucleus. Contributions from SRCs are assumed to be significantly smaller with the contributions falling as the number of high-momentum nucleons increases. Therefore, initial studies of SRCs assumed that only 2*N* SRCs would have significant contributions, and the measurements in these studies focused on scattering from high-momentum nucleons ($k > k_F$) to suppress the contributions from the shell-model structure.

Electron scattering from a stationary proton is kinematically forbidden for energy transfer, ν, below that for elastic *e-p* scattering, corresponding to $x = Q^2/(2M\nu) = 4$. In a nucleus, scattering at $x > 1$ can occur because of the motion of the nucleon in the nucleus, with larger values of x corresponding to larger initial nucleon momenta. Therefore, by selecting scattering at $x > 1$, one can set a minimum initial nucleon momentum that depends on x and Q^2, as shown in **Figure 1*a***. By making the measurements at modest-to-large Q^2 values (>1–2 GeV^2), we minimize FSIs, while the low energy transfer required to reach large x suppresses inelastic scattering. Thus, it was predicted that one might isolate scattering from the high-momentum nucleons in SRCs by requiring x and Q^2 to be large enough that scattering from nucleons below the Fermi momentum would be forbidden (1, 2).

In this region, the inclusive scattering from any nucleus is driven by scattering from 2*N* SRCs generated by the same underlying two-body physics. The scattering in this region should therefore

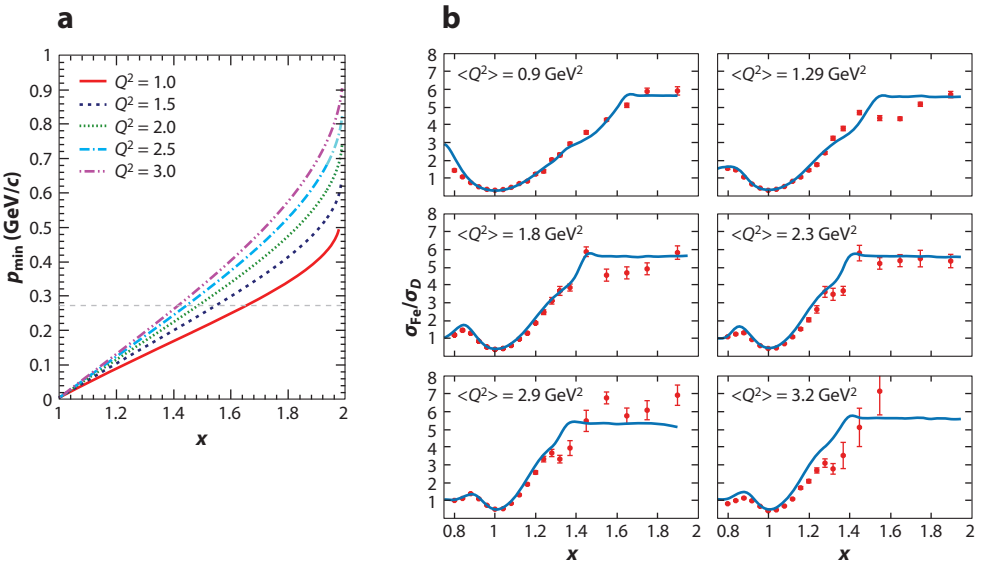

Figure 1

(*a*) Minimum nucleon momentum for quasi-elastic scattering from a nucleon as a function of x and Q^2. (*b*) Fe/*D* inclusive cross-section ratios (per nucleon) from SLAC over a range of Q^2 values. Figure adapted with permission from Reference 16.

show a universal behavior, yielding a nuclear cross-section ratio in the SRC-dominated region that is independent of both x and Q^2. The first extensive set of data to examine this prediction was from SLAC (16), which found a plateau in the A/D cross-section ratio for $x > 1.4$ and $Q^2 > 1.4$ GeV^2 for ^{3}He, ^{4}He, ^{12}C, ^{27}Al, ^{56}Fe, and ^{197}Au. The results for the Fe/*D* ratios are shown for a range of Q^2 values in **Figure 1*b***. High-momentum nucleons ($k > k_F$) are accessible at lower values of x as Q^2 increases, as seen in **Figure 1*b***, yielding a larger plateau region in the high-Q^2 A/D ratios. These data confirmed the prediction of identical behavior in light and heavy nuclei as a function of x and Q^2 for measurements made in the SRC-dominated region, supporting the naive SRC model. Taking the cross section for scattering from SRCs in heavy nuclei to be identical to scattering from a deuteron, the quantity a_2—the A/D ratio in the plateau region—was taken as an approximate measure of the contribution of SRCs relative to that in the deuteron.

At very large Q^2, x can be directly equated with a specific minimum nucleon momentum, while going to lower Q^2 yields a reduction in the range of nucleon momenta associated with the fixed value of x. Thus, the use of x as a proxy for the initial nucleon momentum is an approximation at lower Q^2 values, yielding a Q^2 dependence in the region where the scattering is not dominated by SRCs. This Q^2 dependence can be largely removed by using the light-cone variable α_i, rather than x, as a surrogate for nucleon momentum. The light-cone momentum fraction α_i is analogous, but it is calculated for a bound nucleon in a nucleus, representing a fraction of the total nuclear momentum carried by the nucleon on the light cone. The general form is $\alpha_i = \frac{p_{i\_}}{p_{A\_}/A}$, where $p_{i\_}$ and $p_{A\_}$ are the longitudinal components of the momentum on the light cone for the bound nucleon and for the nucleus, respectively. In the case of a 2*N* SRC, the expression becomes

$$\alpha_{2N} = 2 - \frac{q_{\min} + 2M}{2M}\left(1 + \frac{\sqrt{W^2 - 4M^2}}{W}\right), \qquad 1.$$

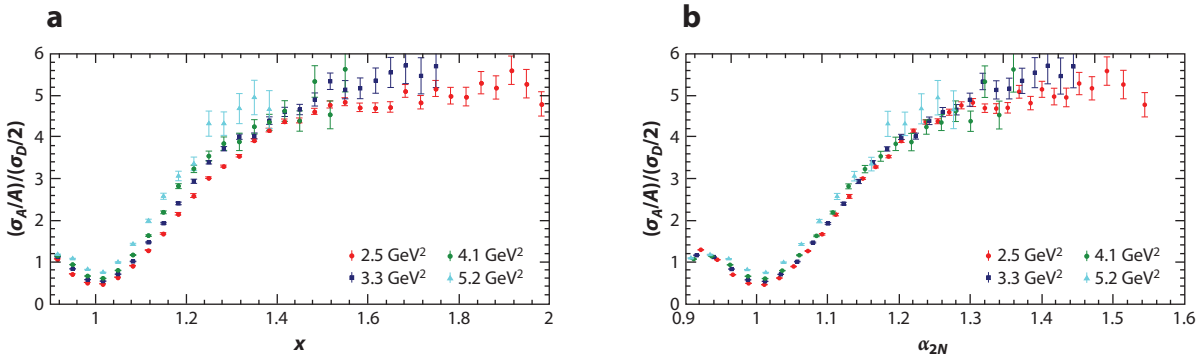

Figure 2

$^{12}C/D$ per-nucleon cross-section ratios plotted (*a*) as a function of x and (*b*) as a function of α_{2N} (15). Q^2 values for $x = 1$ for the different data sets are shown in panels *a* and *b*. The data are nearly independent of Q^2 as a function of α_{2N}.

where $q_{\min} = \nu - |\vec{q}|$, $W^2 = \sqrt{-q^2 + 4M\nu + 4M^2}$, and M is the proton mass. When the $2N$ SRC cross-section ratios are examined as a function of α_{2N} rather than x, as shown in **Figure 2**, the Q^2 dependence is largely removed, and the onset of scaling is more consistent. Note that for $x \approx 1$, the larger values of Q^2 indicate deviations from scaling even when shown versus α_{2N}, as the large inelastic contributions start to become significant in the cross section. Because the larger smearing in heavy nuclei increases the inelastic contributions, the A/D ratio increases for $x \approx 1$ and large Q^2, leading to the increase in the ratio.

Once scaling of the cross sections is observed, there are a few remaining obstacles to quantifying the contribution of SRCs in these nuclei. A common concern is the effect of FSIs, which, despite falling off quickly with increasing Q^2, can have a lingering effect. Most calculations agree that the FSIs at large Q^2 are limited to interactions between the nucleons in the SRC pair and, as such, cancel in the cross-section ratios at $x > 1$ (1, 2, 4, 16–18). This assumption is applied universally in the interpretation of the inclusive ratios in terms of SRC contributions. High-precision $x > 1$ inclusive deuteron data from Jefferson Lab Hall C (Reference 15) were used to extract the underlying momentum distribution at several kinematic settings based on the *y*-scaling approach, which assumes no FSI. The results across settings were consistent and showed no Q^2 dependence in the extracted momentum distributions, even in the SRC-dominated region. In the presence of large FSIs for $x > 1.4$, the momentum distribution would be distorted, which was not observed. While this finding suggests that the effect of FSIs is small, it is difficult to set a precise limit given, among other things, the uncertainty in the strength of the momentum distribution for $k > k_F$.

Having established that the inclusive ratios can isolate and quantify the presence of SRCs in nuclei, later Jefferson Lab experiments compared heavy nuclei with ^{3}He in the SRC region (19, 20) and made precision measurements of A/D ratios in SRC kinematics for a range of light and heavy nuclei (15, 21). In the naive SRC model, these measurements directly provide a relative measure of the cross section in the SRC-dominated region and enable comparison of the strength of SRCs in various nuclei. However, there are corrections to the naive SRC model that have to be addressed for a quantitative interpretation of SRCs, as described in the next subsection.

2.3. Nuclear Dependence of Short-Range Correlations

Scaling of inclusive A/D cross-section ratios at $x > 1$ (15, 16, 21) was taken to signify the presence of high-momentum nucleons born in SRCs. This ratio, taken in the scaling region (which depends on kinematics), is referred to as a_2. However, a_2 was also extracted from $A/^3$He ratios (19, 20)

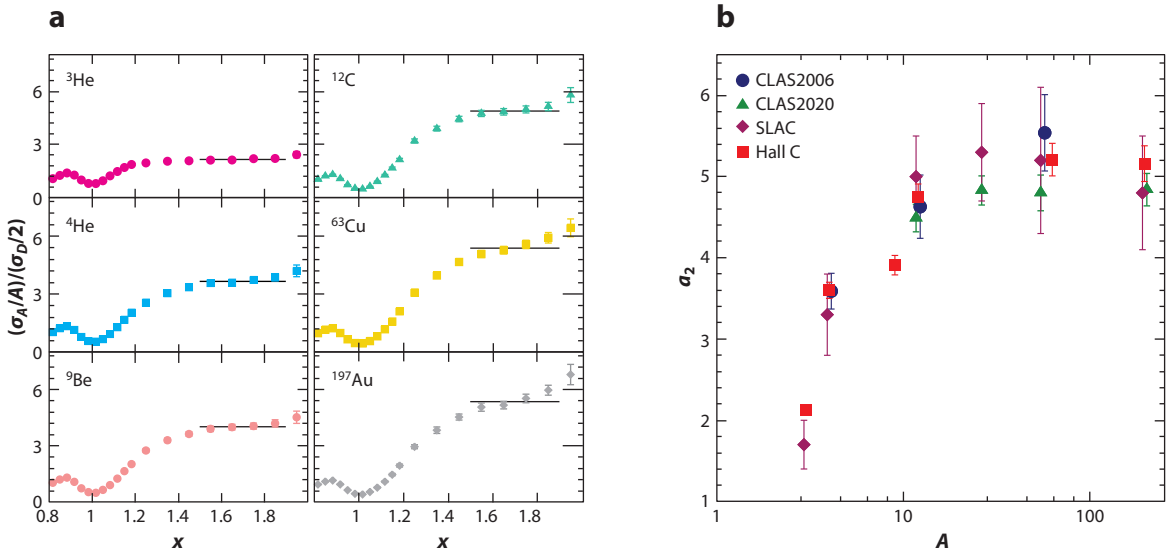

Figure 3

(*a*) Cross-section ratios from Jefferson Lab Experiment E02-019 (15). (*b*) Extracted values of a_2 versus A from all measurements (15, 16, 20, 21); some values have been offset slightly in A to make the results more visible. Note that smearing corrections are estimated to decrease the relative number of short-range correlations from the extracted a_2 value by about 10% for ^{3}He and by about 20% for $A \geq 12$ (15).

combined with ^{3}He/D data and/or calculations to identify the contribution of SRCs relative to the deuteron. **Figure 3*a*** shows the A/D ratios for a wide range of nuclei from Reference 15. One can see that the scaling sets in earlier for light nuclei, while heavier nuclei require larger x to isolate nucleons with momenta above the larger Fermi momentum associated with heavy nuclei.

The extracted values of a_2 from all inclusive measurements are shown in **Figure 3*b*** with the $A/^3$He ratios converted to $A/^2$H using $^3\text{He}/^2\text{H} = 2.12 \pm 0.06$ (the average of data from References 15 and 16). While there are some systematic disagreements between different data sets, they do not appear to be significant given the sizes of the uncertainties, especially since there will be a scale uncertainty on all measurements from a given data set associated with the use of a common set of deuterium data (or ^{3}He for Reference 20). Early works assumed that a_2 would scale with the average nuclear density (or $A^{-1/3}$ as an approximation to nuclear density), but the results of Reference 15 showed that ^{9}Be was an outlier (22) from this model, and the details of the nuclear structure are important. For heavier nuclei, the ratio is approximately consistent, suggesting an effect that saturates in heavy nuclei with roughly 5 "nearest neighbors" able to generate SRCs with any given nucleon (implying roughly 10 "nearest neighbors," only half of which are available to form SRCs assuming *np* dominance). However, because the heavier nuclei have significant neutron excess, it is difficult to cleanly separate A dependence from isospin effects for medium- to heavy-mass nuclei.

Some inclusive SRC ratio measurements (19, 20) assumed equal probability for all isospin SRC pairs (*nn*, *np*, *pp*). Thus, those data for nonisoscalar nuclei were corrected for the a_2 determination. While heavier nuclei also have *pp* and *nn* SRCs, their contributions are significantly smaller, as discussed in Section 3.2. Therefore, the data presented in **Figure 3** are shown without the isoscalar corrections to the cross sections that were applied in some works to account for *pp* and *nn* contributions (19). It is worth noting that the momentum distribution for nucleons in *np* SRCs

is very different from that in *pp* SRCs (23); this issue becomes more important when attempting quantitative comparisons of inclusive scattering, which integrates over a range of initial nucleon momenta, and exclusive reactions, which measure the ratio as a function of initial momentum. This issue is discussed in more detail in Sections 3.2.1 and 3.2.2.

There has been significant theory work aimed at modeling the contribution of 2*N* SRCs as a function of *A* and estimating the relative contributions of *np* SRC and *pp*(*nn*) SRCs. A naive starting point is the total number of *np* pairs ($N \times Z$) or *pp* pairs [$Z \times (Z-1)/2$], but the ratio in the high-momentum tails must be proportional to the overall number of *np* and *pp* pairs, as the tensor interaction generates hard interactions between nucleons in isospin zero states (23–26) (as discussed in detail in Section 3.2). Thus, associating SRCs with pairs of specific spin and isospin states provides a better approximation to the data (27). These simple scaling models can be compared with values of a_2 extracted (23, 28, 29) based on comparing high-momentum (or short-distance) parts of realistic nuclear structure calculations (23, 26, 27, 30–33). Such approaches yield qualitatively consistent results: a significant dominance of *np* SRCs or *pp* and *nn* SRCs and a weak dependence of the total contribution and *np*/*pp* ratio in $A \geq 12$ nuclei. Note that while we focus on an interpretation of SRCs and their isospin structure at the hadronic level, based on the *NN* interaction, a quark-level model explains *np* dominance by associating SRCs with diquark correlations between neighboring nucleons (34), with the ratio of *pp* to *np* SRCs depending on the contributions of three-quark and diquark–quark contributions in the nucleon.

A more quantitative examination of the *A* dependence requires going beyond the assumptions of the naive SRC model as a number of effects may make the *A*/*D* cross-section ratios (a_2) differ from the relative number of 2*N* SRC pairs. The general argument for inclusive measurements is that the cross-section strength at $x > 1$ is due to the presence of high-momentum nucleons from short-range interactions. Thus, the high-momentum tail of the momentum distribution (which is probed at $x > 1$) should look similar across nuclei, with $A > 2$ tails looking approximately like rescaled $A = 2$ tails. One therefore expects the signature of 2*N* SRCs to be a plateau in the cross-section ratios, which is what is observed in the data (see **Figure 3**). However, there are small deviations from a perfectly flat plateau, such as a small increase as one approaches $x = 2$, which are more visible in heavier nuclei. A couple of mechanisms are at play here. One involves the motion of the SRC pair in the field of the other nucleons (discussed below). Another possibility is that at larger *x* there may start to be 3*N* SRC contributions in the region where the 2*N* SRC contributions are dropping off. The 3*N* SRC contribution, relative to that of 2*N* SRCs, is expected to grow with the size of the nucleus (35), leading to increasingly imperfect scaling ratios.

A major correction comes from the center-of-mass (CM) motion of the 2*N* SRC pair in $A > 2$ nuclei. This modifies the shape of the momentum distribution and redistributes strength (from the QE peak to the high-momentum tail). The first data to be corrected for this effect were those of Reference 15. The authors calculated the effect of this smearing using parameterizations of the $F(y)$ scaling function convolved with realistic parameterizations for the CM motion from Reference 18. The correction was on the order of 20% for most nuclei, with a low value of 10% for ^{3}He. A more recent work (36) examines the same effect in relativistic and nonrelativistic convolution models, using the generalized contact formalism (GCF) to provide the structure of the SRCs to be smeared, and also examines the impact of having a larger excitation of the residual $(A-2)$ system. However, Reference 36 does not provide direct comparisons of calculations with and without SRC smearing or $(A-2)$ binding, making it difficult to determine the size of the individual effects.

Below, we typically refer to a_2 as a measure of the relative contribution of SRCs, consistent with most of the literature, although efforts are ongoing to better quantify the corrections between the cross-section ratios and the relative SRC contributions.

3. INTERNAL STRUCTURE OF SHORT-RANGE CORRELATIONS

In addition to mapping out the size of the SRC contributions in nuclei, various experimental studies have focused on obtaining a more detailed understanding of the structure of SRCs in nuclei. Such work addresses some of the questions raised by the initial inclusive measurements: What is the isospin structure of SRCs, what is the momentum distribution of SRCs in nuclei, and what is the distribution of relative momenta within SRCs? Finally, as SRCs represent virtual excitations resulting from strong, short-distance interactions, is the internal structure of nucleons modified by being in these dense, energetic configurations?

While the inclusive measurements were able to confirm SRC contributions by identifying the universal behavior in all nuclei in the (x, Q^2) range predicted by the SRC model, the earlier measurements were sensitive mainly to the overall contribution from SRCs. They did not provide information on the isospin structure of the SRCs—the relative contribution of *pp*, *np*, and *nn* SRCs—and did not measure the momenta of SRCs in nuclei. In both cases, corrections had to be applied based on assumptions or measurements of the isospin structure and momentum distribution of SRCs. Below, we discuss our understanding of these effects and their experimental and theoretical support.

3.1. Measurements of Center-of-Mass Motion of Short-Range Correlations in Nuclei

Theoretical predictions and experimental results suggest that the typical momentum of the CM of an SRC pair is small (i.e., on the order of mean-field momenta) (26). Nevertheless, determining the CM motion distribution of pairs has important implications. As noted in Section 2.3, the inclusive measurements have to apply a correction for the motion of the SRCs inside the nucleus to extract the relative SRC contributions in different nuclei. Furthermore, the CM momentum distribution may shed some light on how SRCs form. So far, experiments have aimed to quantify the width of the CM momentum distribution and have assumed a Gaussian shape, which is broadly consistent with the data given the available statistics and resolution. For what follows, we use the following convention: For two nucleons in an SRC pair with momenta $\vec{p}_1$ and $\vec{p}_2$, the CM momentum is defined by $\vec{p}_{\rm CM} \equiv \vec{p}_1 + \vec{p}_2$, while the relative momentum is $\vec{p}_{\rm rel} \equiv \frac{1}{2}(\vec{p}_1 - \vec{p}_2)$.

Experimental determinations have been made through $2N$ knockout reactions. One of the earliest such measurements was performed by colliding a 6- to 9-GeV proton beam from a fixed carbon target in the Brookhaven EVA spectrometer and identifying SRC breakup events from the ^{12}C(*p*, *ppn*) reaction (37). Guided by theoretical indications that the transverse directions would be far more sensitive to FSIs, Tang et al. (37) measured the longitudinal component of the CM distribution to have a Gaussian width of 143 ± 17 MeV/*c* (i.e., somewhat smaller than the Fermi momentum). Electron scattering experiments using the spectrometers in Jefferson Lab's Hall A measured a width of 136 ± 20 MeV/*c* in the (*e*, *e*′*pp*) channel for carbon (38) and a smaller width of 100 ± 20 MeV/*c* for ^{4}He in the (*e*, *e*′*pn*) channel (39). In both cases, the small acceptances of the spectrometers required that the CM width be inferred from the measured distribution using a simulation in which the electron scattered from a nucleon in a moving pair. The result was obtained by matching the data and simulated distributions.

Measurements on a number of different nuclei have been made at CLAS, where the large acceptance is advantageous for reconstructing a multinucleon final state. References 40 and 41 reported measurements of ^{3}He(*e*, *pp*)*n* and used these data to study both the relative and CM momenta of the nucleons in SRCs. Reference 42 made similar measurements for additional nuclei and found that *pp* SRCs could be well described as having Gaussian CM momentum distributions with widths ranging from 143 ± 7 MeV/*c* for ^{12}C to 157 ± 14 MeV/*c* for ^{208}Pb. These results

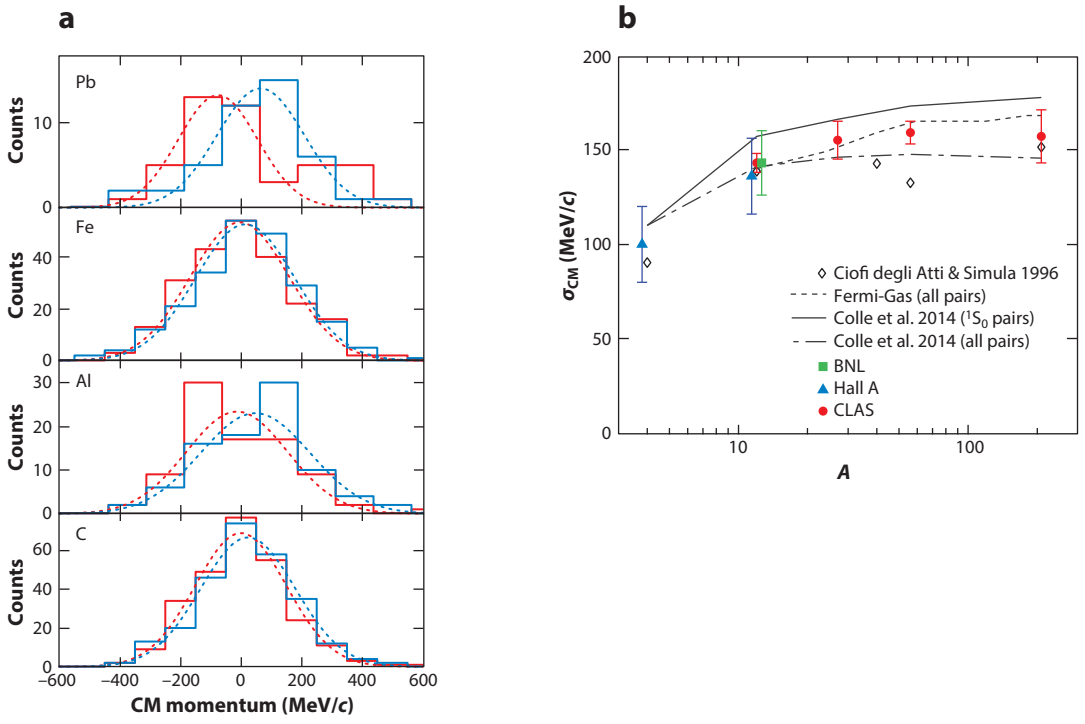

Figure 4

(*a*) Proton–proton SRC CM momentum distributions from Reference 42 in the direction transverse to p_m in the *x* (*red*) and *y* (*blue*) directions, before correcting for the CLAS acceptance. (*b*) The Gaussian width associated with SRC motion in nuclei extracted in Reference 42 compared with calculations from References 18 and 27, and a Fermi gas prediction from Reference 42 based on values from Reference 43. Abbreviations: CM, center of mass; SRC, short-range correlation.

were generally consistent with the widths assumed based on mean-field momenta of the nuclei. A summary of these results is shown in **Figure 4*a***.

3.2. Isospin Structure of Short-Range Correlations

As we discuss in the following sections, a series of measurements has made it clear that 2*N* SRCs are dominated by *np* SRCs, meaning that the isospin structure of SRCs is nearly identical for all nuclei, and the scattering from an SRC is roughly proportional to the sum of the *e*-*p* and *e*-*n* cross sections.

While early inclusive measurements neglected the isospin structure of SRCs, the comparison of heavy nuclei with the deuteron will be affected by the presence of *pp* and *nn* SRCs, which is not possible in the deuteron. As noted in Section 2.3, some measurements applied corrections to the cross section per nucleon to correct for the difference between the elastic *e*-*p* and *e*-*n* cross sections.

Multiple approaches have been used to study the isospin structure of SRCs. As noted in Section 2, $A(e, e'p)$ measurements are challenging to interpret at high missing momenta. The first measurements examining the isospin structure used detection of both the struck nucleon from the SRC and its spectator partner. Although in this approach one has to worry about large FSI corrections, certain contributions will cancel in the comparison of *np* and *pp* final states. Additional studies using $A(e, e'p)/A(e, e'n)$ at large and small missing momenta and recent inclusive

studies making use of the isospin structure of the target support the picture of *np* dominance; each approach has its own advantages and limitations.

3.2.1. Two-nucleon knockout measurements. Information about the isospin structure of SRCs can be directly accessed in measurements in which both correlated nucleons are detected. Such measurements face a couple of experimental challenges. First, since the detection of neutrons is accomplished differently than that of protons, care must be taken to control the relative acceptance and efficiency between the two particles. Second, as with all measurements with a nucleon in the final state, FSIs are important. For these measurements, the results are particularly sensitive to charge-exchange reactions (where an outgoing proton knocks out a spectator neutron or vice versa) or scattering from a low-momentum nucleon that rescatters from a spectator nucleon, generating a final state that is identical to scattering from a preexisting SRC. Different experiments have used a variety of strategies to negotiate these challenges, and while these issues affect the quantitative interpretation, the body of experimental data clearly points to the dominance of *np* SRCs in the momentum range of ∼300–600 MeV/*c*. The evolution of isospin structure at higher momenta is an area of active research.

The first estimate of the isospin structure of SRC pairs was made using ^{12}C(*p*, *ppn*) and ^{12}C(*p*, *pp*) data collected by the EVA spectrometer at Brookhaven National Laboratory; the investigators found that correlated protons were accompanied by the emission of back-to-back neutrons 92^{+8}_{-18}% of the time (44). This was confirmed by an electron scattering experiment in Jefferson Lab Hall A, in which high-resolution spectrometers were used to detect the scattered electron as well as a knocked-out proton in high-p_m kinematics, while a third spectrometer was used to look for recoiling protons and neutrons. The *pp* pair fraction was inferred from both the ^{12}C(*e*, *e*′*pp*)/^{12}C(*e*, *e*′*p*) (38) and ^{12}C(*e*, *e*′*pp*)/^{12}C(*e*, *e*′*pn*) ratios (45). The results of these measurements are shown in **Figure 5*a***. A follow-up measurement confirmed *np* dominance for the ^{4}He nucleus (39).

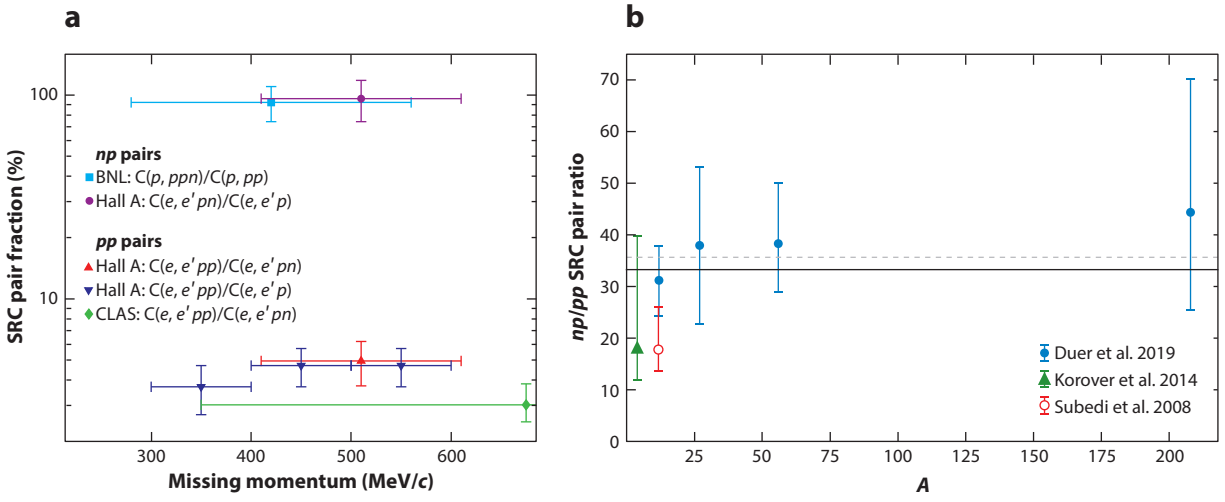

Figure 5

(*a*) The *pp* SRC and *np* SRC fractions as a function of missing momentum from References 38, 44, 45, and 47. Panel adapted with permission from Reference 45. (*b*) *np*/*pp* SRC pair ratio from direct measurements using 2*N* knockout (39, 45, 47). The solid line indicates the average ratio including the Subedi et al. (45) point, which signicantly underestimated (47) the FSI corrections, and the dashed line indicates the average ratio excluding the Subedi et al. (45) point. Abbreviations: FSI, final-state interaction; SRC, short-range correlation.

An analysis from the CLAS Collaboration considered *np* dominance in nonisoscalar nuclei (46). Since the CLAS system had limited capabilities for neutron detection, inferences were drawn from a measurement of the $A(e, e'pp)/A(e, e'p)$ ratio. To compensate for the number of undetected recoil protons, double ratios were formed relative to carbon. The results showed that in aluminum, iron, and lead, *pp* correlations yield only a small contribution to the high-momentum proton distribution, with the rest assumed to be generated by *np* SRCs, as previously observed in carbon. The contribution of *pp* pairs decreases slightly in aluminum, in iron (relative to carbon), and more significantly in lead, though the uncertainties are large and the data are also consistent with no decrease. A follow-up analysis in which $A(e, e'np)$ events were identified via neutron hits in the CLAS electromagnetic calorimeter had consistent findings (47). Note that the FSI corrections applied in this work were substantially larger than those applied in the initial measurement at Jefferson Lab (38), yielding a result ~70% larger than that of the initial work. **Figure 5*b*** shows the ratio of *np* SRCs to *pp* SRCs extracted from all direct 2*N* knockout measurements.

The measurements described above have looked at scattering from nucleons in correlated pairs, with the possible additional detection of a spectator. By contrast, an analysis of ^{3}He$(e, e'pp)n$ data at CLAS was performed in kinematics where the spectator pair was correlated while the struck nucleon was not (41). Events with *pp* and *np* pairs were identified by relative energy transfer among the detected protons and undetected neutrons. This analysis confirmed the relative scarcity of *pp* pairs while also observing that the effect diminishes for large pair CM momentum (41). It is not clear whether this is a result of the details of the $A = 3$ wave function, is caused by final-state effects, or is produced by some other phenomenon.

3.2.2. Single-nucleon knockout. One can also attempt to study the isospin structure of SRCs using 1*N* knockout. One technique is to compare relative rates of proton and neutron knockout in high-p_m kinematics. A CLAS analysis of $(e, e'p)$ and $(e, e'n)$ in both correlated and mean-field kinematics was undertaken to study the asymmetry dependence of pairing (48). It was found that while the $(e, e'n)/(e, e'p)$ ratio in mean-field kinematics scales roughly with N/Z (after correcting for the difference between the elastic *e-p* and *e-n* cross sections), this ratio is approximately unity in SRC kinematics, a clear sign of *np* dominance persisting in asymmetric nuclei. The relative abundance of nucleons in correlated and mean-field states, that is, $(e, e'N)_{SRC}/(e, e'N)_{MF}$, was also studied for both protons and neutrons. Since the relative acceptance for the two kinematics was very different, a double ratio relative to carbon was used. It was found that the fraction of correlated protons steadily increases with N/Z, while the double ratio remains flat for neutrons. In a simple *np*-dominance picture, the neutron ratio would have a slight decrease.

Isospin structure can also be tested in isospin mirror nuclei, that is, where the behavior of protons in one nucleus can provide information about the neutrons in the other. An $(e, e'p)$ experiment was conducted in Jefferson Lab Hall A on ^{3}H and ^{3}He pairs with a goal of mapping the relative momentum distribution for protons and neutrons in the $A = 3$ system. The measurement was conducted in antiparallel, $x > 1$ kinematics for p_m in the range of 50 to 500 MeV/*c*, that is, across the transition from the conventional mean field to the correlated regimes. The ratio ^{3}He$(e, e'p)/^3$H$(e, e'p)$ (49) was measured to be above 2 at low missing momentum and fell to approximately 1.4 at $p_m = 250$ MeV/*c*, consistent with the onset of *np* dominance and also with PWIA calculations based on three-body spectral functions (50). However, for even larger missing momenta, the ratio rose again, inconsistent with PWIA predictions. An analysis of the absolute cross sections showed that while the $x > 1$ kinematics goes a long way to reducing FSIs, it can still affect the measured cross-section ratio, particularly through charge-exchange reactions, which can increase the helium $(e, e'p)$ cross section and decrease the tritium $(e, e'p)$ cross section with a nontrivial p_m dependence

(51). While the general result is in agreement with the *np*-dominance picture, detailed FSI calculations are necessary to draw firm quantitative conclusions about the nuclear ground state.

3.2.3. Inclusive studies on nonisoscalar nuclei. Because inclusive scattering is sensitive to both proton and neutron knockout, the cross section is proportional to a combination of *np*, *pp*, and *nn* SRCs. In general, this means that there is little sensitivity to the isospin structure of the SRCs, especially in scattering from isoscalar nuclei, and deviations from simple models of the A dependence associated with neutron excess do not provide sufficient sensitivity to look for isospin dependence. This is in part because the effects are not large, but also because it is difficult to separate the A dependence from the N/Z dependence given that the deviation of N/Z tends to grow with mass in nuclei for which SRC measurements exist. However, by comparing scattering from targets with similar mass but different isospin structure, one can attempt to isolate the isospin structure of the SRCs.

The first such experiment compared ^{48}Ca and ^{40}Ca scattering in 2N SRC kinematics (50). These nuclei have similar mass and should therefore have nearly the same total contribution from *NN* SRCs, but ^{48}Ca should have an excess of *nn* SRCs relative to *pp* SRCs due to the additional neutrons. Because the *e-n* cross section is lower than the *e-p* cross section, this would yield a decrease in the cross section per nucleon in 2N SRC kinematics unless *np* and *pp* SRCs have negligible contributions. Taking into account the small difference in the expected SRC contribution for $A = 40$ and $A = 48$ and the ratio of the *e-p* to *e-n* cross section, the ^{48}Ca/^{40}Ca per-nucleon cross-section ratio was predicted to yield 0.975 in the case of 100% *np* SRCs and 0.930 for isospin-independent SRC formation (50). The measurement observed a ratio of 0.971(12), corresponding to near-total *np* dominance, with 2σ and 1σ lower limits on the *np*/*pp* enhancement factors of 2.9 and 10.6, respectively. This confirmed the observation from 2N knockout measurements while avoiding the need for large FSI corrections. However, given the very small difference between the predictions for isospin independence and *np* dominance, potential corrections to the assumptions used to interpret the data could affect the quantitative interpretation.

More recently, a comparison of scattering from mirror nuclei ^{3}H and ^{3}He was performed (52), which has several advantages over the measurement using calcium isotopes. First, because ^{3}H and ^{3}He structure are nearly identical, there is next to no correction for the difference in nuclear structure apart from the isospin structure. Second, because the fractional change in N/Z is much larger between the two nuclei, there is a much larger difference for the prediction of the ^{3}H/^{3}He cross-section ratio in the SRC regime: 0.74 for isospin independent versus 1 for *np* dominance. This suggests that the measurement will be almost an order of magnitude more sensitive to the relative contribution of *pp* SRCs.

3.3. Short-Range Correlation Internal Momentum Distributions

While the previous section has discussed the ratio of *np*/*pp* SRCs in aggregate, some experiments have demonstrated that this ratio varies as a function of p_{m} (39, 53, 54), suggesting a difference in the relative internal momentum distribution for *np* and *pp* SRCs. Such a difference has been seen in ab initio calculations of the *np* and *pp* pair distributions in nuclei (23–26). As such, a more detailed understanding of the role of SRCs has to include study of the internal structure of the SRCs, which generates the observed p_{m} dependence. While many experiments aim to extract ratios of SRCs (between nuclei, or the ratio of *np* to *pp* pairs), the measurements are sensitive to the cross-section-weighted contribution of those pairs over the p_{m} range of the measurement, not just a number of pairs in the nucleus that is universal in all measurements. Comparisons of different measurements must account for differences in kinematic coverage or in the probe being used. These challenges

call for a more nuanced approach that models the internal momentum distribution of SRCs, such as the GCF (see Section 3.3.1).

In addition, measurements that include detection of one or more nucleons in the final state need to account for FSIs. Even in a mean-field model where there are no SRCs in the initial state, simple rescattering can generate a measurement with a leading struck nucleon and a second high-momentum nucleon (above the Fermi momentum), which are indistinguishable from scattering from an SRC pair in the initial state. In addition, charge-exchange rescattering can be an exceptionally large correction, in particular when trying to isolate the very small *pp* SRC contributions from the much larger *np* SRC contributions.

3.3.1. Generalized contact formalism. One challenge to interpreting the results of $2N$ knockout measurements has been, until recently, the lack of theoretical cross-section calculations with which to compare results. While there are methods for calculating the breakup of deuterium and $A = 3$ nuclei, and $1N$ spectral functions for heavier nuclei, calculations of the full $2N$ knockout decay function for nucleons in short-range correlated pairs have proved difficult. For that reason, several recent analyses have turned to the GCF, a factorized model of SRCs within a nucleus, to calculate fully differential $2N$ knockout cross sections to compare with data. A theoretical derivation of the GCF can be found in Reference 55, but the core concept is the assumption that at asymptotically short-distance or high-momentum scales, the nuclear wave function Ψ can be factorized:

$$\Psi_{r_{ij}\to 0} \longrightarrow \sum_{\alpha} \varphi_{\alpha}(\mathbf{r}_{ij}) A_{ij}^{\alpha}(\mathbf{R}_{ij}, \{\mathbf{r}_{k\neq ij}\}), \qquad 2.$$

where $\mathbf{r}_{ij}$ is the separation vector between nucleons i and j, $\mathbf{R}_{ij}$ is their CM coordinate, α represents the set of possible quantum numbers of a pair of nucleons, φ represents a universal two-body wave function that is independent of the nucleus, and A_{ij}^{α} represents the wave function of the remaining $A-2$ nucleons. A similar formulation can be written in momentum space. Over these asymptotic scales, A_{ij}^{α} is approximately constant, and one can define the contact matrix:

$$C^{\alpha,\beta} = 16\pi^2 N_{ij} \langle A_{ij}^{\alpha} | A_{ij}^{\beta} \rangle, \qquad 3.$$

where N_{ij} is the number of possible pair combinations. Numerous selection rules determine which off-diagonal elements can be nonzero, and in practice one considers only the diagonal terms, referred to as the contacts, C^{α}, which can be interpreted as the abundance of short-range correlated pairs with quantum numbers α in a nucleus.

The asymptotic behavior of the nucleons within a correlated pair is determined by the universal functions $\varphi_{\alpha}(\mathbf{r}_{ij})$ in position space or $\tilde{\varphi}_{\alpha}(\mathbf{k}_{ij})$ in momentum space. These functions can be estimated from a given model *NN* potential by solving for the zero-energy solution to the two-body Schrödinger equation (56). While different model *NN* potentials lead to different universal functions, comparisons with ab initio variational Monte Carlo (VMC) calculations confirm the asymptotic behavior predicted by the GCF as well as the universality of pair behavior across different nuclei (29). Comparison with VMC calculations is one of the ways that values of the contacts, that is, the SRC pair abundances, can be estimated (29, 56).

In addition to modeling properties of pairs within nuclei, the GCF can be used to predict the fully differential cross section for the knockout of SRC nucleons. This is especially powerful for $2N$ knockout, where the differential cross section has three extra differential dimensions. In $1N$ knockout, the cross section within the PWIA can be factorized:

$$\mathrm{d}^6\sigma \sim K\sigma_{eN} S(E_{\mathrm{m}}, \mathbf{P}_{\mathrm{m}}), \qquad 4.$$

where K is the kinematic factor, σ_{eN} is the cross section for the electron to scatter elastically from an off-shell nucleon, and $S(E_m, \mathbf{p}_m)$ is the spectral function that describes the probability of finding a nucleon within a nucleus with momentum equal to the missing momentum, $\mathbf{p}_m$, and separation energy equal to the missing energy, E_m. In $2N$ knockout, the spectral function is supplanted by the $2N$ decay function (57):

$$d^8\sigma \sim K'\sigma_{eN} D(E_m, \mathbf{p}_m, \mathbf{p}_r), \quad 5.$$

where K' is a different kinematic factor and $D(E_m, \mathbf{p}_m, \mathbf{p}_r)$ additionally describes the probability for a second recoil nucleon to be ejected with momentum $\mathbf{p}_r$. In the GCF, the decay function can be written in a factorized form:

$$D(E_m, \mathbf{p}_m, \mathbf{p}_r) = \sum_\alpha C^\alpha \left|\tilde{\varphi}^\alpha\left[\frac{1}{2}(\mathbf{p}_m - \mathbf{p}_r)\right]\right|^2 P^\alpha_{CM}(\mathbf{p}_m + \mathbf{p}_r)\delta(m_A - E_1 - E_r - E_{A-2}), \quad 6.$$

where $E_1 \equiv E_N - \omega$. In the above equation, $|\tilde{\varphi}^\alpha|^2$ represents a universal, that is, nucleus-independent, two-body momentum distribution for pairs with quantum numbers α. P^α_{CM} represents the CM momentum distribution, which is typically modeled by a Gaussian. A similar equation can be formulated in light-front coordinates (58).

The tunable parameters of Equation 6 are the contact terms C^α, parameters defining the CM momentum distribution (typically a single Gaussian width, σ_{CM}), and finally, any parameters describing the excitation energy of the $A-2$ system (typically denoted by a single average value, E^*). These parameters can be estimated either from the results of ab initio VMC calculations (e.g., 29) or from data.

The usefulness of the GCF for interpreting experiments is wide-ranging, and many new avenues are under active development. First and foremost, the GCF specifies a fully differential cross section for scattering from correlated nucleons. The GCF cross sections can reproduce, in $x > 1$ kinematics, the multidimensional kinematic distributions of $1N$ and $2N$ knockout (54). Such theoretical calculations have been lacking, or have used simpler approximations, in previous SRC studies. Another benefit is that the GCF provides a simple connection to underlying nuclear properties within the model, that is, pair abundances, CM motion, and so forth. The GCF can be used to study the sensitivity measurements of those properties, whether by calculation of various correction factors (58) or by direct inference from data (36). Since the GCF specifies a plane-wave cross section, it can be used to identify the effects of FSIs through significant deviations from data. Lastly, since the model is factorized, it is applicable to reactions other than electron scattering, such as proton scattering in inverse kinematics (59) and photoproduction (60).

3.3.2. Isospin structure at high missing momentum. The GCF has been useful for interpreting the observed p_m dependence of the relative abundance of *pp* and *np* SRCs. Measurements in Jefferson Lab's Hall A (39) and at CLAS (53, 54) have observed an increase in the relative yield of $(e, e'pp)$ events in the p_m range of 500 to 800 MeV/c. Inferring the prevalence of *pp* SRCs from this observation, however, requires correcting for the detector acceptance for recoil protons, which in turn depends on the SRC relative momentum and center-of-mass momentum distributions. Rather than trying to estimate such a correction and its uncertainty due to model dependence, Reference 54 addressed this problem by using a forward-propagated technique: simulating effects including experimental acceptance on scattering events generated according to the cross section predicted by GCF under many different model assumptions. The rise in the observed relative yield of $(e, e'pp)$ was shown to be consistent with a tensor-dominant to scalar-dominant transition predicted by several different *NN* interaction models. Reference 53 added an analysis of $(e, e'pn)$ data, though the statistical uncertainties were too large to observe a corresponding drop

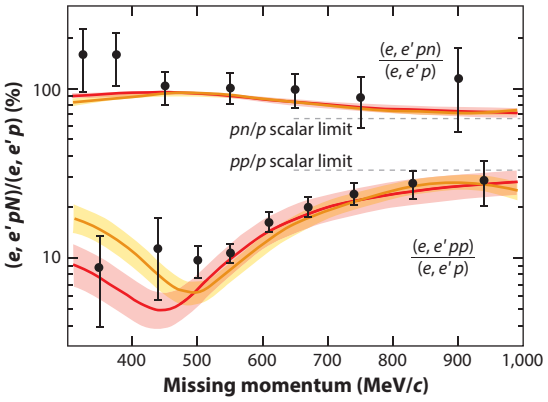

Figure 6

Measured *pn*/*p* and *pp*/*p* fractions compared with generalized contact formalism (GCF) calculation. Figure adapted with permission from Reference 53.

in the relative abundance of *pn* SRCs. The combined results of References 53 and 54 are shown in **Figure 6**, along with the respective GCF predictions for two different *NN* interaction models.

3.4. Impact of Short-Range Correlations on Other Fields of Physics

While 2*N* SRCs are most easily studied in high-energy scattering measurements, their impact on nuclear structure can be seen in neutron stars (61, 62) and ν-*A* scattering (63–65) studies of nuclear structure and ν oscillation. They may also provide insight into nuclear quark distributions and the EMC effect through studies aimed at elucidating the connection between SRCs and the EMC effect (see Section 3.5.1).

The impact of 2*N* SRCs in nuclei can modify *eA*, νA, and *AA* interactions in a way that is not captured in mean-field calculations of the nuclear structure. While ab initio calculations of light nuclei and infinite nuclear matter can consider these contributions, including the observed *np* dominance, this is more challenging for medium- and heavy-mass nuclei. In addition, there are many cases where mean-field calculations that do not include SRC contributions in the scattering observables have been used because of a lack of appropriate ab initio calculations or because the mean-field structure was assumed to be sufficient.

Our present understanding of SRCs provides guidance on the overall strength and isospin structure of their contributions. In many cases, this is sufficient to allow detailed calculations or at least realistic modeling of the contribution from SRCs in other reactions. Where ab initio calculations are not available, or where their input is not directly used in scattering calculations, momentum distributions or spectral functions can be constructed based on a combination of mean-field and SRC contributions (18, 66), although there has been progress recently on extracting structure functions directly from ab initio calculations (26, 67, 68). The GCF (see Section 3.3.1) provides a relatively simple and flexible way of implementing SRCs in structure and scattering calculations.

3.5. Structure of the Nucleons Within Short-Range Correlations

The scale of nuclear binding (tens of MeV) is so much smaller than the GeV energy scales associated with deep inelastic scattering (DIS) measurements that probe the structure function and quark distributions of nucleons and nuclei. Because of this scale separation, it was initially assumed that the quark distributions in a nucleus would be the sum of its constituent proton and neutron

quark distributions with percent-level effects associated with binding and Fermi momentum. The EMC Collaboration first observed (69) that the structure function from iron differed significantly from that of deuteron, taken as an approximation of the free proton and neutron distributions. This observation—that the quark structure of the nucleus has significant deviations from the proton and neutron distributions—was dubbed the EMC effect. Experiments at SLAC (70) expanded these measurements to additional nuclei and showed that this effect was a universal feature of finite nuclei, with the deviation of the nucleus from a simple sum-of-nucleons picture growing with nuclear density (71).

While many explanations have been proposed to explain the EMC effect, as summarized in References 72 and 73, we do not yet have a clear understanding of the underlying physics. Several works have examined in more detail the impact of binding and Fermi motion of the nucleons, nonnucleonic contributions to the nuclear quark distributions (e.g., those carried by virtual pions in the nucleus), and modification of the nucleon structure when bound in a nucleus. While there is a growing consensus that contributions beyond binding and Fermi motion are required (74, 75), additional measurements are needed to better constrain attempts to explain nuclear quark distributions.

Several experiments have been proposed to elucidate the origin of the EMC effect (72, 73, 76). In the following section, we discuss recent ideas that were motivated by Jefferson Lab studies of both SRCs and the EMC effect, as well as the experiments that motivated these new ideas.

3.5.1. EMC-SRC correlation. As noted in Section 2.3, measurements of SRCs in light nuclei (15) showed that the contribution of SRCs in light nuclei deviated significantly from the predictions of the simple scaling models used to describe data in heavier nuclei (71). Models where the SRC contribution scales with average nuclear density failed to describe the anomalously large value of a_2 in ^{9}Be, whose average density is very low, while models that scale with the target mass could not explain the large difference between a_2 in ^{3}He and ^{4}He (22).

The data on SRCs matched the unexpected behavior of the EMC effect (77, 78), showing a nontrivial correlation between the EMC effect and the presence of SRCs. Previously, it had been assumed that both effects scaled with the average nuclear density (71, 72), but the unexpected behavior in light nuclei showed that the EMC effect and the presence of SRCs are sensitive to the detailed nuclear structure. This suggests either that both effects are driven by the same underlying physics or that the EMC effect is driven by the presence of SRCs in nuclei. This commonality has been referred to as the EMC-SRC correlation, and while a great deal of effort has gone into examining the correlation, it is as yet unclear what underlying physics drives the connection between these two observables.

This idea of a connection between the EMC effect and SRCs was first raised in Reference 79, which quantified the correlation and interpreted it as a consequence of the density dependence of both effects. Shortly thereafter, Reference 80 examined this correlation and speculated that the EMC effect was associated with the high virtuality of nucleons in SRCs. At the time, only ^{3}He, ^{4}He, ^{12}C, and ^{56}Fe had measurements of both the EMC effect and SRC contributions, and it was already known that both effects scale approximately with nuclear density or $A^{-1/3}$ (70, 71). It was not until the SRC data on ^{9}Be (15) that there was a common deviation from the simple dependence on density for both the EMC effect and SRCs.

The ^{9}Be EMC effect was initially explained (77) by looking at the local density, as seen by the struck nucleon, rather than the average density of the nucleus. In the local density picture, the α-cluster structure of ^{9}Be yields significantly more overlap between nucleons and a much larger EMC effect than in models assuming that the EMC effect scales with the average nuclear density. Reference 80 described the EMC-SRC correlation as a consequence of the high-momentum

(large-virtuality) nucleons in SRCs. Because the SRCs are generated by nucleons interacting at short distances, there is a connection between the contribution of nucleons at short distances and the number of high-momentum nucleons. This connection makes it difficult to determine whether the EMC effect is driven by short-distance configurations, as in the local density (LD) picture, or by high-momentum SRCs, as in the high-virtuality (HV) picture. In both cases, the cluster structure of ^{9}Be yields short-distance configurations, which would explain the larger-than-expected contribution of SRCs. In the HV approach, the enhanced SRC contribution causes the increased EMC effect, while in the LD picture, the short-distance, high-density clusters yield an enhanced EMC effect as well as an enhanced SRC contribution. Both approaches can explain the correlation, but they may have quantitative differences; for instance, *np* dominance of SRCs would imply that only *np* pairs would generate the EMC effect in the HV picture, whereas in the LD model, all short-distance *NN* pairs could contribute.

Reference 81 reexamined the correlation including the data of Reference 15 and found that the observation of the EMC-SRC correlation was largely independent of what corrections were applied to the data (e.g., corrections accounting for potential isospin structure of the SRCs). The robustness of the correlation is a consequence of the limited precision of the measurements, in particular for the EMC effect, making it difficult to use the correlation to test different hypotheses of the EMC-SRC correlation with the data available at the time. Even so, a quantitative analysis comparing simple models of the correlation for the LD and HV approaches showed a slightly better correlation in the LD picture, but the difference was only at the level of two standard deviations (22).

3.5.2. Potential implication for flavor dependence of the EMC effect. The observed EMC-SRC correlation, combined with the observation of *np* dominance in SRCs, suggests that the EMC effect might have an isospin dependence associated with the excess of high-momentum protons in neutron-rich nuclei. In this case, the fraction of high-momentum protons and neutrons scales as N/A and Z/A, respectively, such that there is an equal number of high-momentum protons and neutrons. This observation suggests that the EMC effect in protons would increase with neutron excess (in neutrons, it would decrease with neutron excess). This would introduce a flavor dependence of the EMC effect with enhanced modification of the *u* quark distributions in neutron-rich nuclei. Note that a flavor-dependent EMC effect is also a natural consequence of looking individually at the proton and neutron distributions, whether one assumes that the EMC effect is driven by high virtuality, by local density, or even by different overlap between protons and neutrons (e.g., in a neutron-rich nucleus with a neutron skin) (28).

Such a flavor dependence is difficult to observe in inclusive EMC effect measurements because the neutron excess tends to increase with the mass of the nucleus, and the existing data make it difficult to separate an A dependence from an N/Z dependence in heavy nuclei. However, an extension of the analysis mentioned above (22) was performed in which it was assumed that only *np* SRCs contribute to the EMC effect, thus providing a specific flavor dependence for the EMC effect and allowing for the extraction of a "universal" EMC effect for the *np* SRCs (21). The investigators extracted their proposed universal modification function, under the assumptions noted above, and found that it was largely independent of A. They concluded that it was in fact a universal function with a flavor-dependent EMC effect driven by the isospin structure of *np* SRC dominance.

Shortly thereafter, another analysis compared the universal function based on *np* SRC dominance (HV approach) with an equivalent function based on the LD model, where all *NN* pairs at short distance contribute (analogous to the comparison of the EMC-SRC correlation assuming HV or LD in Reference 22). The results are shown in **Figure 7*a*** (HV) and **Figure 7*b*** (LD).

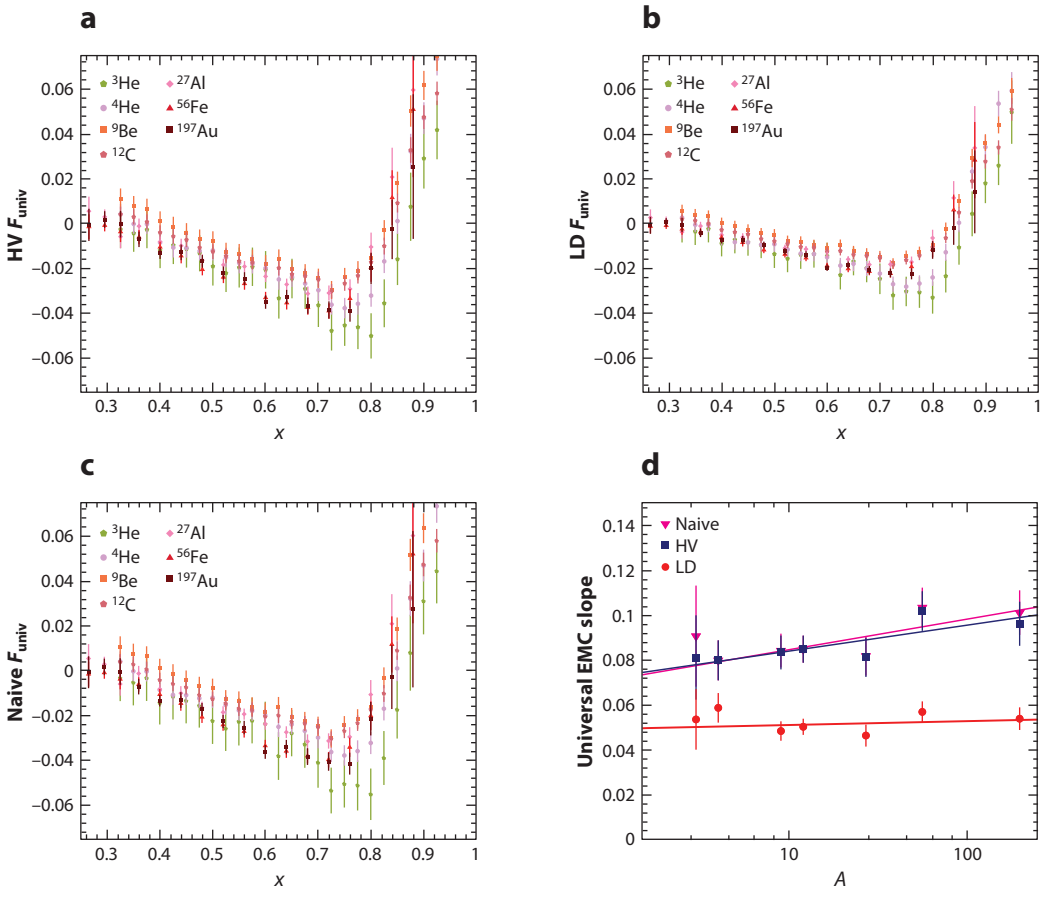

Figure 7

Three versions of the universal deuterium EMC effect function: (*a*) HV and (*b*) LD functions of Reference 82 and (*c*) the naive universal function with no explicit isospin dependence (EMC effect for each nucleus scaled down by its measured value of a_2). (*d*) Comparison of the slopes from each of the universal functions for the data from References 70, 77, and 78. Abbreviations: HV, high virtuality; LD, local density.

While the exact form of the isoscalar corrections applied to the data differed slightly from that described in Reference 21, the universal function based on the HV assumption (*np* dominance) was nearly identical to the result of Reference 21. The LD-based universal function, assuming a flavor-independent EMC effect, showed a more consistent EMC slope as a function of A. Examining the A dependence of the universal functions (**Figure 7*d***), the LD model was more consistent with the hypothesis of A independence, but only at the level of two standard deviations.

Figure 7*c* shows the slopes from a third version of a universal modification function based simply on the observation of the EMC-SRC correlation. In this case, the universal function is obtained by scaling down the nuclear EMC effect (deviation of the structure function ratio from unity) by the factor a_2 with no assumptions about the underlying cause or flavor dependence. For isoscalar nuclei, this is equivalent to the HV universal function from Reference 21, while for the nonisoscalar nuclei, it has an extremely small impact on the slope of the universal EMC function, as seen in **Figure 7*d***. As such, the data have little direct sensitivity to the explicit assumption of flavor dependence in the HV-based universal function compared with the naive model of a

flavor-independent EMC effect that scales with a_2. The difference between the HV and LD functions does not come directly from the explicit flavor-dependent effect; instead, it comes from the fact that the LD model takes a_2 as a relative measure of the contribution of *np* SRCs and then scales from the number of *np* pairs (NZ) in the nucleus to the total number of *NN* pairs [$A(A-1)/2$]. This scaling factor, $A(A-1)/(2NZ)$, yields an A dependence even for isoscalar nuclei and gives a reduced A dependence in the universal EMC slope. However, an implicit assumption is that all *NN* pairs contribute equally at short distances, while the short-distance distributions for *pp*, *np*, and *nn* pairs can differ. Thus, these comparisons are useful in examining the impact of certain assumptions on the extracted size of the EMC effect in the deuteron, but the data have limited sensitivity even in the extreme/simplified cases assumed in such analyses. Future experiments (83, 84) will improve the situation by measuring the contribution of SRCs and the EMC effect for a variety of light nuclei and for medium-to-heavy nuclei covering a range of N/Z; the resulting data set will enable better separation of the A dependence and the N/Z dependence of the EMC effect.

3.5.3. Impact on other physics. Whether the EMC effect is flavor dependent (and, if so, how large the effect is) is an important question that relates to both the origin of the EMC effect and the matter of obtaining reliable quark distributions for both nonisoscalar nuclei and the neutron. **Figure 7*d*** shows a smaller universal EMC effect for the deuteron—by almost a factor of 2 based on the average of all nuclei and by a factor of 1.5 if the behavior is extrapolated to the deuteron using the fits shown. This difference is significant in the extraction of the neutron structure function (85, 86) and quark distributions (87, 88) from comparisons of proton and deuteron structure functions. In addition, it was pointed out in Reference 22 that a flavor dependence of the EMC effect in nonisoscalar nuclei would affect the extraction of the neutron structure function from comparisons of ^{3}H and ^{3}He (89), and initial examinations of the impact of such a flavor dependence using the data from Reference 89 have already appeared (90, 91).

In addition, high-energy scattering or collider experiments (eA, νA, or AA) with heavy neutron-rich nuclei are sensitive to the difference between the EMC effect for protons and neutrons. A reliable analysis of such data will require an understanding of the modification of up and down quarks in nonisoscalar nuclei. In addition, polarized ^{3}He is often used as an effective polarized neutron target as the spins of the protons cancel almost completely. However, if used for DIS studies of the polarized parton distribution functions (PDFs) of semi-inclusive DIS (SIDIS), a flavor-dependent EMC effect will yield an additional correction that is currently neglected in such analyses. Furthermore, the fact that the neutron polarization is largely associated with lower-momentum nucleons (26) means that the flavor-dependent EMC effect may differ from the unpolarized EMC effect both in x dependence and in sensitivity to the part of the ^{3}He wave function sampled in the experiment.

Thus, the question of whether only *np* SRCs or all short-distance pairs contribute to the EMC effect has a significant impact on nuclear PDFs, the predicted EMC effect for the deuteron, and spin structure studies on ^{3}He. Note that the question of flavor-dependent versus flavor-independent effects is not the same as the question of local density versus high virtuality. The LD hypothesis can yield a flavor-dependent or flavor-independent EMC effect, depending on the isospin structure in nucleon pairs at small separations. However, it is typically taken to be flavor independent to allow a comparison with models that include an explicit flavor dependence. In addition, other ideas have been proposed to make direct measurements of the flavor dependence of the EMC effect in pion-induced Drell–Yan scattering (92), SIDIS (93, 94), and parity-violating electron scattering (95, 96). A review of ideas and future plans to more fully understand the EMC effect can be found in Reference 76.

4. THREE-NUCLEON SHORT-RANGE CORRELATIONS

So far, we have focused on 2*N* SRCs, where only two nucleons interact to produce large relative but small total momenta. Short-range configurations with more than two nucleons are not prohibited, but they are expected to occur with decreasing probability. Following searches for 2*N* SRCs, attempts were also made to observe a second plateau in nuclear cross-section ratios relative to ^{3}He. The first observation claim, published by the CLAS Collaboration (20), showed a second plateau starting at $x \approx 2.25$ (see **Figure 8**). This was surprising because the Q^2 value was low (average of 1.7 GeV^2) and the onset of scaling was low in x. Other experiments were carried out (15, 97) with high-resolution spectrometers to examine the Q^2 dependence of the second plateau as well as its nuclear dependence. The results from Jefferson Lab's Hall C E02-019 experiment (15) are inconclusive; the data are consistent with a plateau, but the uncertainties in the region of interest are large. However, the ratio is significantly higher than what was observed by the CLAS Collaboration, and the would-be plateau starts later in x (which aligns better with expectations), contradicting the interpretation of the CLAS data in terms of isolating 3*N* SRCs. A follow-up Jefferson Lab Hall A experiment (97) performed a scan over Q^2, including the CLAS kinematics, but failed to observe a 3*N* plateau, as can be seen in **Figure 8**. The plateau initially observed in Reference 20 was later shown to be an effect of bin migration, where all the $x > 2.2$ bins came from a single E' bin (98). Thus, we still have no definitive experimental observations of 3*N* SRCs, and the question of whether there is a kinematic region where they dominate the scattering remains open.

While the onset of the 2*N* SRC plateau has well-defined kinematics, the picture is less clear for 3*N* SRCs because there are multiple possible configurations, as shown in **Figure 9**. Three nucleons can share three units of momentum equally (symmetric configuration), which would result in nucleons with high momenta comparable to those in a 2*N* configuration. A highly asymmetric configuration is also possible. While we can calculate $p_{\min}$ as a function of x and Q^2 for heavy nuclei, this value is dependent on the momentum distribution of the spectators in the 3*N* SRC, so a more realistic estimate of relevant minimum momenta for 3*N* SRCs is dependent on the symmetric and asymmetric momentum configurations.

Another difficulty arises because the contribution from 2*N* SRCs falls off more slowly than the mean-field contributions, and so predicting what nucleon momentum is required for the 3*N* SRCs to dominate (and result in a second plateau) depends on the size and nature of the 3*N*

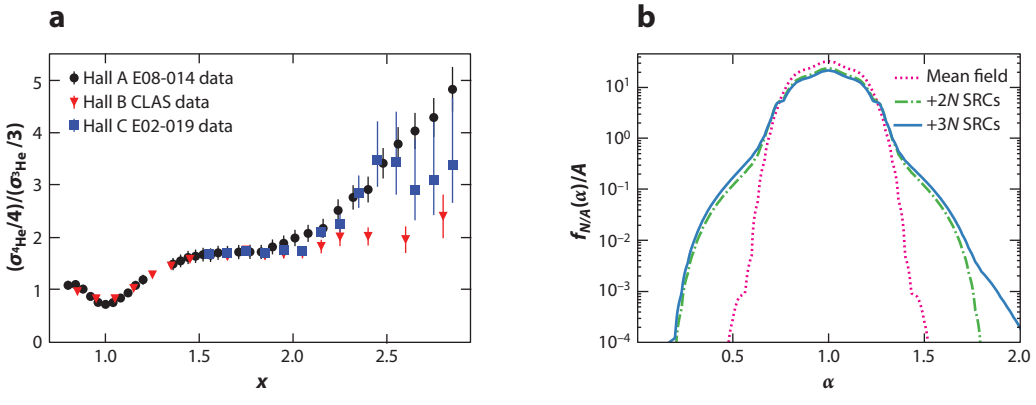

Figure 8

(*a*) ^{4}He/^{3}He per-nucleon cross-section ratio versus x (15, 20, 97). (*b*) Calculation of the mean-field, 2*N* SRC, and 3*N* SRC contributions from Reference 99. Abbreviation: SRC, short-range correlation.

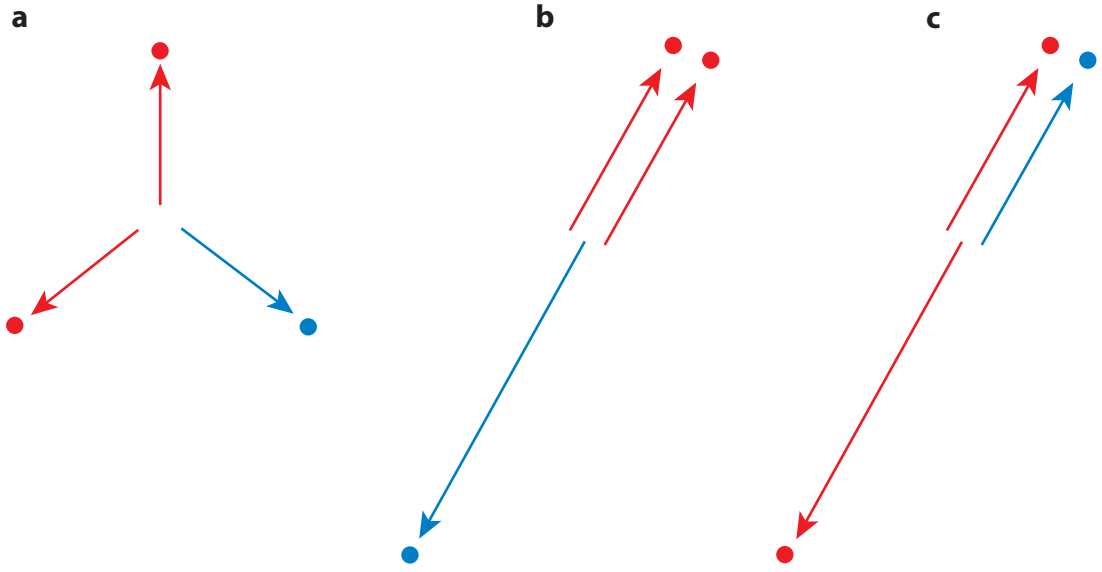

Figure 9

Different potential momentum-sharing and isospin configurations for (*a*) symmetric and (*b*, *c*) asymmetric 3*N* short-range correlation configurations.

SRC contributions. Furthermore, the structure of the 3*N* SRC is more complicated, and predictions regarding its contribution are highly model dependent. Results of one such calculation are shown in **Figure 8*b***, with the star configuration assumed for a 3*N* SRC (99). In this model, the 3*N* SRC contribution begins to have a significant contribution at $\alpha \approx 1.5$, but it does not dominate until $\alpha \approx 1.8$. While the transition from mean-field to 2*N* SRC dominance is clear, given the rapid and well-understood falloff of the mean-field momentum distribution, the transition to 3*N* SRCs depends strongly on both the 2*N* SRC and 3*N* SRC structures assumed in the calculations. Based on this calculation, it was argued that 3*N* SRCs might be visible somewhere above $\alpha = 1.6$ (35), corresponding to $x = 2.3$ for the E02-019 data (15), with all other data sets stopping before $\alpha = 1.6$. While the ratio is consistent with a plateau for $x > 2.3$, the statistics are limited, and data exist for only one Q^2, meaning that this data set is not sufficient to identify universal three-body behavior in ^{3}He and ^{4}He. Reference 35 also predicts that $a_3(A)$, the $A/^3$He ratio in the 3*N* SRC region, should go like a_2^2 (neglecting isospin differences), and the E02-019 data are consistent with this prediction. Thus, there are hints that $\alpha = 1.6$ might be sufficient to study 3*N* SRCs, but new data at higher Q^2 are needed to confirm the presence of 3*N* SRCs (83, 100).

The 3*N* SRC landscape is further clouded by the possibility of multiple isospin configurations. If we expect some analog with the 2*N* SRC, where there is a region of *np* dominance, there should be *ppn* and *pnn* dominance among 3*N* SRC configurations. Even if SRCs are dominated by *ppn* and *pnn* contributions (as opposed to three of a kind, which could be less probable, as *pp* and *nn* are in 2*N* SRCs), scattering from isoscalar nuclei should have identical contributions from these configurations (plus possible configurations from *ppp* or *nnn* SRCs). Previous and upcoming measurements have used the ^{3}He nucleus for the measurement in the denominator, as it is the smallest stable nucleus with three nucleons. However, in ^{3}He, only the *ppn* 3*N* SRC configuration is possible, meaning the a_3 ratio will be sensitive to differences in the number of protons and neutrons at the largest momenta in 3*N* SRCs.

In a symmetric configuration (**Figure 9*a***), scattering from the highest-momentum nucleons in ^{3}He will involve both protons and the neutron. In a highly asymmetric configuration (**Figure 9*b*,*c***), the high-momentum part of the distribution could be dominated by the singly occurring neutron, the doubly occurring proton, or some combination. Thus, the question of whether the highest-momentum nucleons are protons, neutrons, or a mix of both will modify the $A/^3$He ratio. If the relative contributions of protons and neutrons vary as a function of momentum, this could also distort the x dependence of the ratio. Future Jefferson Lab 12-GeV measurements (83, 100) should shed light on many of these questions.

5. KEY QUESTIONS AND FUTURE DIRECTIONS

In this review, we have tried to highlight recent progress in our understanding of the short-range structure of nuclei, describing key discoveries and important insights from theory. Here, we summarize some of these key points and discuss the remaining physics questions that will complete our picture of SRCs and their impact on nuclear structure at both the hadronic and partonic levels. Plans to expand on previous measurements and novel probes of SRCs aimed at addressing these remaining questions are presented below.

5.1. Summary of Our Understanding of Short-Range Correlations and Remaining Questions

Inclusive measurements identified kinematic regions of 2N SRC dominance in nuclei, confirming the predictions for the kinematic region where SRCs should dominate and observing the expected universal two-body behavior through scaling in x and Q^2. Such measurements mapped out the A dependence of the contribution of SRCs, identifying ^{9}Be as an outlier from the expected scaling with density and indicating that understanding SRCs requires a microscopic picture of the nuclear structure.

SRC measurements also showed an intriguing correlation with measurements of the EMC effect, raising questions about the flavor dependence of the EMC effect. However, only the ^{9}Be data indicate that this correlation goes beyond simple scaling of both effects with nuclear density, and the direct sensitivity of both SRC and EMC measurements to isospin structure is limited by the finite number of measurements on nuclei with neutron excess and by the fact that the neutron excess tends to grow with mass in heavier nuclei, making it difficult to separate mass- and isospin-dependent effects.

Triple-coincidence measurements have given us insight into the isospin structure of 2N SRCs, showing an enhancement of np SRCs over pp and nn SRCs at the ∼30:1 level in all nuclei measured. This observation has been confirmed in a variety of measurements, with new results to come for ^{3}H and ^{3}He (29, 52).

While 2N SRCs have been identified and quantified, and significant progress has been made in understanding their momentum and isospin structure, we do not yet know what (if any) role 3N SRCs play in nuclear structure. Whereas early measurements suggested that they had been observed (20), later experiments (15, 101) did not agree with the initial observation, which is now believed to have been limited by the experimental momentum resolution (98). Because each of these experiments had one or more significant limitations—low Q^2 values, poor statistics, insufficient resolution—an argument can be made that there has yet to be a meaningful test of the 3N SRC hypothesis.

Based on the discussion above, we identify the following as key questions that require further data and insight to be fully answered.

- How can we improve direct, quantitative comparisons of different measurements of $2N$ SRCs, and how well can we constrain calculations by combining the results of these different experiments?
- What is the contribution of $3N$ SRCs, and what is their internal momentum and isospin structure?
- What is the origin of the EMC-SRC correlation, and what does it imply for the internal structure of nucleons in SRCs and the flavor dependence of the EMC effect?

5.2. Extensions of the Current Experimental Program

Several planned experiments will extend the type of SRC studies we have discussed above. These include experiments that will make measurements on new targets, expanding the kinematic coverage to higher x or Q^2, or provide improved statistics. We summarize these experiments below, and in Sections 5.3–5.5 we discuss new and novel measurements that will probe SRCs and their internal structure in completely new ways.

5.2.1. Two-nucleon short-range correlation and EMC effect measurements in new nuclei. Two experiments are scheduled to run in 2022 that will measure A/D ratios to extract the contribution of SRCs (83) and the EMC effect (84) in a wide range of nuclei. These will include several light nuclei—^{3,4}He, ^{6,7}Li, ^{9}Be, ^{10,11}B, and ^{12}C—to look at the A dependence of both effects in these well-understood nuclei. In addition, these experiments will study medium-to-heavy nuclei over a range of N/Z and attempt to disentangle the A dependence and isospin dependence of SRCs and the EMC effect. This work will also provide a better data set to examine the impact of isospin structure on the EMC-SRC correlation.

5.2.2. Three-nucleon short-range correlations. One of the abovementioned experiments (84) will also perform the first significant search for $3N$ SRCs and will provide the first data with large enough Q^2 values and high enough precision to clearly observe a plateau in x at $x > 2$, if it exists, as discussed in Section 4. Depending on what is observed, further measurements could be performed (100) to confirm the Q^2 independence of the scattering and to map out the A dependence. In addition, measurements on ^{3}H and ^{3}He could provide a sensitive probe of the momentum/isospin structure of $3N$ SRCs, even if inclusive scattering does not allow for a clean isolation of $3N$ SRC contributions (94, 100).

5.2.3. Two-nucleon knockout. The nuclear targets program at CLAS-12 (102), which began data collection in 2021, will leverage the larger acceptance, higher luminosity and data rate, and increased neutron detection capabilities of CLAS-12 to pursue higher-statistics studies of $2N$ knockout. Combined with improved modeling of reaction effects and FSIs, this program will refine our understanding of isospin structure, momentum structure, size, and asymmetry dependencies of SRCs, with the additional goal of detecting $3N$ knockout events.

A number of new programs will use different probes to test the degree to which reaction effects factorize from the nuclear structure. A 2021 experiment using the GlueX spectrometer aims to identify SRCs in $2N$ knockout using photoproduction (60). A program of inverse kinematics measurements has begun at the Joint Institute for Nuclear Research in Dubna, Russia, using beams of nuclei incident on proton targets. The advantage of this technique is that the residual nucleus and correlated spectator nucleons have significant momentum in the lab frame, facilitating detection and momentum analysis. For example, the detection of an intact boron nucleus in the breakup of SRC pairs in carbon has been shown to reduce apparent final-state effects (59). This technique

could open the possibility of studying SRCs in unstable nuclei, for instance, at the future FAIR Facility.

In addition to these measurements, which represent natural extensions of the already-completed studies, other new measurements may provide significant new information and allow us to better understand the microscopic structure of SRCs and the origin of the EMC effect. While there are several possibilities for new measurements that can help identify the origin of the EMC effect (76), we provide three examples below that are more directly related to the connection between the EMC effect and SRCs.

5.3. New Directions: Partonic Structure and Nonnucleonic Degrees of Freedom

The existing inclusive studies have demonstrated that it is possible to isolate scattering from SRCs by going to sufficiently large x values at modest-to-large Q^2 values. By extending to much higher Q^2, but maintaining sufficiently large x, it should be possible to stay in the SRC-dominated regime while making DIS measurements to probe the target's quark distributions. In this way, we can study the nuclear PDFs at $x > 1$ and extract the distribution of so-called superfast quarks in nuclei (1, 3). In this region, where SRC contributions should be large, different models make very different predictions for the superfast quark distribution. This might also provide a way to test quark-level descriptions of SRCs, for instance, where SRCs are associated with diquark correlations between neighboring nucleons (34).

The first such proposed measurement should take data in 2022 (83), with Q^2 values from 15 to 20 GeV^2 for x up to 1.4. Such a measurement should be extremely sensitive to certain types of more exotic configurations within nuclei. Early examinations of the EMC effect looked at the contribution of six-quark bags as a model for exotic configurations for which the quark momentum distributions would be significantly modified. A small (5%) contribution from six-quark bags would have very little impact on the structure function in the DIS region, at most 1–2% (83), as illustrated in **Figure 10*a***. However, the free momentum sharing between six quarks carrying twice the longitudinal momentum of a single nucleon yields a large (fractional) enhancement for $x > 1$,

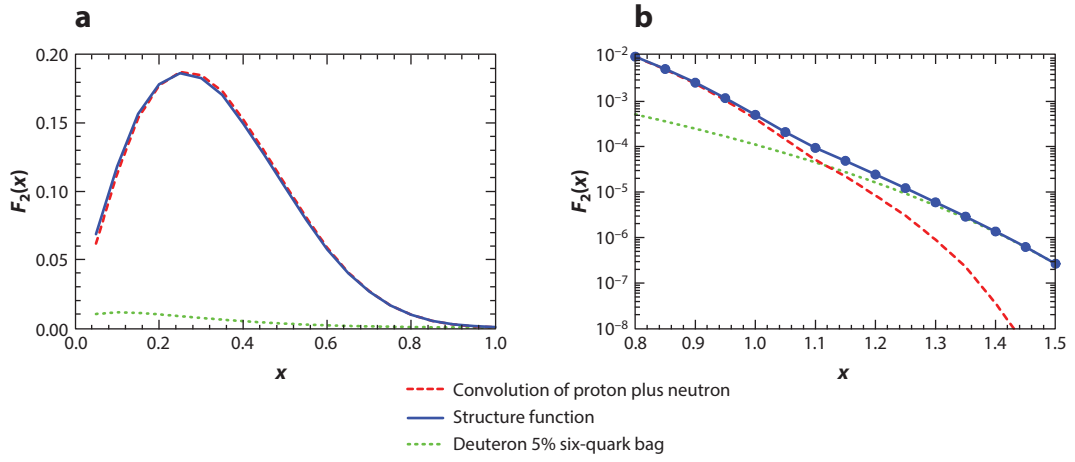

Figure 10

(*a*) Plot showing the calculated valence deuteron structure function based on convolution of proton plus neutron (*red dashed line*) versus the structure function (*blue solid line*) where the deuteron includes a 5% component of a six-quark bag (106) (*green dotted line*). (*b*) The same functions plotted on a logarithmic scale focused on $x > 1$.

matching or even significantly exceeding the contributions that come from Fermi smearing. Thus, a percent-level modification for the deuteron PDF for $x < 0.8$ could yield an order-of-magnitude enhancement over the PDFs obtained from a simple convolution of a proton and neutron, as illustrated in **Figure 10*b***. While this estimate was made using a six-quark bag model (3, 83, 99, 103), any enhancement of momentum sharing between overlapping nucleons would be expected to yield a qualitatively similar effect. Models where the EMC effect is driven by highly virtual nucleons show a significant suppression of the structure function for off-shell as opposed to on-shell nucleons at large x and light-cone momentum α (104). DIS at $x > 1$ requires $\alpha > 1$, as shown in figure 35 of Reference 5, allowing for a measurement that does not directly tag α for the nucleon but that is still sensitive to the large-x nucleon PDFs at $\alpha > 1$, where significant suppression of the free nucleon structure function is predicted by several models (5, 104, 105).

One critical aspect of such a measurement will be demonstrating sensitivity to the PDFs at $x > 1$, where the conventional kinematics criteria for DIS scattering on a nucleon do not apply. The data taken at 6 GeV were limited to $Q^2 < 10$ GeV^2, and yet they were well reproduced by a QCD-inspired fit (107). The 12-GeV measurement (83) will extend these measurements to $Q^2 \approx 20$ GeV^2, making them more appropriate for an analysis in terms of the nuclear quark distributions. In addition, if nonnucleonic contributions yield a very large deviation from the simple proton plus nucleon convolution, the effect should be clear as long as the data are DIS dominated, even if they are not purely DIS.

One can also make measurements that are explicitly aimed at identifying nonnucleonic degrees of freedom including hidden color configurations (108–110) through measurements of $A(e, e'N\Delta)$ or $A(e, e'\Delta\Delta)$. In the presence of such nonnucleonic configurations at short-distance scales, there would be a significant enhancement of SRC-like $N\Delta$ or $\Delta\Delta$-like pairs (111). Initial estimates suggested that such measurements would be much more sensitive at 12 GeV or even higher energies.

5.4. New Directions: Flavor-Dependent EMC Effect

As noted in Section 3.5.2, the EMC-SRC connection raised the question of whether the EMC effect is flavor dependent, in particular for nonisoscalar nuclei. This will be examined by measurements of the EMC effect for nonisoscalar nuclei (e.g., ^{40}Ca and ^{48}Ca), but as shown in **Figure 7**, the flavor dependence associated with the neutron excess in heavy nuclei has only a modest impact on the EMC effect. While a direct measurement of sufficient sensitivity does not appear to be possible, the systematic study of Jefferson Lab Experiment E12-10-008 (84) may allow for a model-dependent separation of A and isospin dependence.

The use of SIDIS to flavor-tag scattering on nuclei has been proposed as a way to examine the flavor dependence of the EMC effect (93, 94). However, measurements in heavy nuclei, where the expected effects are likely to be relatively significant, have to deal with model-dependent corrections and other possible nuclear effects, which may make it difficult to cleanly isolate the flavor dependence of the nuclear PDFs. These issues can be addressed by going to light nuclei, in particular in a comparison of ^{3}H and ^{3}He, but it is not clear that realistic models of the flavor dependence will be large enough to measure in such experiments.

A clean and sensitive measurement can be performed using parity-violating electron scattering on nonisoscalar nuclei (95). This involves looking for a modest change in a parity-violating asymmetry of order 100 parts per million, and while this is within the capabilities of modern parity-violating measurements, it requires high luminosity and large acceptance as well as good control of false asymmetries. This appears to be within the capabilities of the SoLID detector planned for parity-violating DIS measurements at Jefferson Lab (112), and a proposal was submitted to

perform such a measurement on ^{48}Ca (96) that can provide excellent sensitivity to estimates of the flavor dependence based on simple scaling models (28) or the calculations of Reference 95.

5.5. New Directions: Tagged Measurements of Short-Range Correlations

Another approach related to flavor dependence is the technique of spectator tagging, especially in deuterium, whereby the detection of a recoiling spectator nucleon can identify the struck nucleon and provide information about the deuteron's initial configuration (i.e., short range versus long range). The requirement of nucleon detection makes the technique sensitive to FSIs, though theoretical estimates indicate that the effects are smallest when the spectator recoils in the backward direction (113, 114). This technique is used in the BoNuS experiment at CLAS, in which the detection of a low-momentum spectator proton indicates that the accompanying DIS reaction took place on a neutron. By extrapolating to a stationary neutron limit, the BoNuS experiment aims to determine the structure of the free neutron. First results were published in 2011 from the 6-GeV program (115–117). A subsequent 12-GeV measurement is currently under analysis (118).

Whereas the BoNuS experiment is focused on slow-moving spectators, two other Jefferson Lab experiments aim to detect high-momentum (300–600 MeV/c) spectators as a way of determining the structure modification in SRC pairs, thus testing models of the EMC effect. The BAND experiment (119) took CLAS data in 2019 with a backward-angle detection system added to measure backward-recoiling spectator neutrons. The Jefferson Lab Hall C LAD experiment (120) will detect recoiling spectator protons. Both experiments aim to determine how nucleon structure modification changes with virtuality. Their combined results may give an indication of how bound proton modification differs from that of the bound neutron. Such studies can be extended to higher energy and larger spectator momenta at the proposed Electron-Ion Collider (121).

5.6. Summary and Conclusions

Over the past few decades, extensive sets of data related to SRCs have become available, mainly from the Jefferson Lab experimental program. With these data in hand, we have mapped out the contribution of SRCs over a range of nuclei and measured their isospin and momentum structure. Overall, enough has been learned that we are in a position to incorporate this short-distance physics into nuclear structure calculations related to low-energy scattering, neutrino–nucleus scattering, and neutron star structure. These new data have driven significant experimental progress in quantifying SRCs and understanding their internal structure, although more work is required to understand FSIs and the momentum structure of np and pp SRCs well enough to make detailed, quantitative comparisons of different measurements that are sensitive to SRCs. Beyond these developments, the issue of 3N SRCs remains unanswered: What is their isospin and momentum structure, and can they be isolated experimentally? These questions are important enough that studies of SRCs and related high-energy nuclear structure measurements continue to be a significant part of the future Jefferson Lab experimental program (122).

Beyond the direct measurements of SRCs in nuclei, this experimental program has also raised questions that touch on other aspects of high-energy nuclear structure, such as whether the EMC-SRC correlation represents a commonality of origin or a direct causal connection by which SRCs generated modified nucleon structure because of their short-distance and/or high-momentum nature. The possibility of a causal connection, combined with the strong np dominance of 2N SRCs, suggests a flavor-dependent EMC effect in nonisoscalar nuclei. This motivates further studies of the EMC effect as well as a program of studies to probe the internal partonic structure of SRCs, either through DIS measurements at kinematics that isolate

scattering from SRCs or from tagged measurements that look at the nucleon structure (effective form factors or PDFs) as a function of nucleon virtuality.

Answering these questions will require not only the experimental program described in this review but also improvements in the theory necessary to interpret the measurements. Improved FSI corrections are needed for more quantitative studies in 1*N* and 2*N* knockout reactions, and the extraction of the modification of the nucleon structure through tagged measurements of effective form factors or PDFs relies on careful comparison with calculations that account for both the conventional nuclear effects and the modification of the nucleon structure within SRCs. Close collaboration has driven the simultaneous advancement of both experimental data and theoretical understanding and will continue to open up new avenues for future study.

DISCLOSURE STATEMENT

The authors are not aware of any affiliations, memberships, funding, or financial holdings that might be perceived as affecting the objectivity of this review.

ACKNOWLEDGMENTS

The authors wish to thank Wim Cosyn, Adam Freese, Shujie Li, Augusto Machiavelli, and Jerry Miller for useful discussions and other contributions. This work was supported in part by the Department of Energy's Office of Science, Office of Nuclear Physics, under contracts DE-AC02-05CH11231, DE-SC0013615, and DE-SC0016583.

LITERATURE CITED

1. Frankfurt LL, Strikman MI. *Phys. Rep.* 76:215 (1981)
2. Frankfurt LL, Strikman MI. *Phys. Rep.* 160:235 (1988)
3. Sargsian MM, et al. *J. Phys. G* 29:R1 (2003)
4. Arrington J, Higinbotham DW, Rosner G, Sargsian M. *Prog. Part. Nucl. Phys.* 67:898 (2012)
5. Hen O, Miller GA, Piasetzky E, Weinstein LB. *Rev. Mod. Phys.* 89:045002 (2017)
6. Fomin N, Higinbotham D, Sargsian M, Solvignon P. *Annu. Rev. Nucl. Part. Sci.* 67:129 (2017)
7. Egiyan KS, et al. *Phys. Rev. Lett.* 98:262502 (2007)
8. Boeglin WU, et al. *Phys. Rev. Lett.* 107:262501 (2011)
9. Sargsian MM. *Phys. Rev. C* 82:014612 (2010)
10. Benhar O, Day D, Sick I. *Rev. Mod. Phys.* 80:189 (2008)
11. Day DB, et al. *Phys. Rev. Lett.* 59:427 (1987)
12. Arrington J, et al. *Phys. Rev. Lett.* 82:2056 (1999)
13. Ciofi degli Atti C, West GB. *Phys. Lett. B* 458:447 (1999)
14. Arrington J. In *Baryons 2002: Proceedings of the 9th International Conference on the Structure of Baryons*, ed. CE Carlson, BA Mecking, pp. 567–70. Singapore: World Scientific (2003)
15. Fomin N, et al. *Phys. Rev. Lett.* 108:092502 (2012)
16. Frankfurt LL, Strikman MI, Day DB, Sargsian M. *Phys. Rev. C* 48:2451 (1993)
17. Ciofi degli Atti C, Simula S. *Phys. Lett. B* 325:276 (1994)
18. Ciofi degli Atti C, Simula S. *Phys. Rev. C* 53:1689 (1996)
19. Egiyan KS, et al. *Phys. Rev. C* 68:014313 (2003)
20. Egiyan KS, et al. *Phys. Rev. Lett.* 96:082501 (2006)
21. Schmookler B, et al. *Nature* 566:354 (2019)
22. Arrington J, et al. *Phys. Rev. C* 86:065204 (2012)
23. Schiavilla R, Wiringa RB, Pieper SC, Carlson J. *Phys. Rev. Lett.* 98:132501 (2007)
24. Alvioli M, Ciofi degli Atti C, Morita H. *Phys. Rev. Lett.* 100:162503 (2008)
25. Wiringa RB, Schiavilla R, Pieper SC, Carlson J. *Phys. Rev. C* 78:021001 (2008)
26. Wiringa RB, Schiavilla R, Pieper SC, Carlson J. *Phys. Rev. C* 89:024305 (2014)

27. Colle C, et al. *Phys. Rev. C* 89:024603 (2014); Colle C, et al. *Phys. Rev. C* 92:024604 (2015)
28. Arrington J. *EPJ Web Conf.* 113:01011 (2016)
29. Cruz-Torres R, et al. *Nat. Phys.* 17:306 (2021)
30. Feldmeier H, Horiuchi W, Neff T, Suzuki Y. *Phys. Rev. C* 84:054003 (2011)
31. Ryckebusch J, Cosyn W, Vanhalst M. *J. Phys. G* 42:055104 (2015)
32. Mosel U, Gallmeister K. *Phys. Rev. C* 94:034610 (2016)
33. Ryckebusch J, Cosyn W, Vieijra T, Casert C. *Phys. Rev. C* 100:054620 (2019)
34. West JR. arXiv:2009.06968 [hep-ph] (2020)
35. Sargsian MM, Day DB, Frankfurt LL, Strikman MI. *Phys. Rev. C* 100:044320 (2019)
36. Weiss R, et al. *Phys. Rev. C* 103:L031301 (2021)
37. Tang A, et al. *Phys. Rev. Lett.* 90(4):042301 (2003)
38. Shneor R, et al. *Phys. Rev. Lett.* 99:072501 (2007)
39. Korover I, et al. *Phys. Rev. Lett.* 113:022501 (2014)
40. Niyazov RA, et al. *Phys. Rev. Lett.* 92:052303 (2004). Erratum. *Phys. Rev. Lett.* 92:099903 (2004)
41. Baghdasaryan H, et al. *Phys. Rev. Lett.* 105:222501 (2010)
42. Cohen EO, et al. *Phys. Rev. Lett.* 121:092501 (2018)
43. Moniz EJ, et al. *Phys. Rev. Lett.* 26:445 (1971)
44. Piasetzky E, et al. *Phys. Rev. Lett.* 97:162504 (2006)
45. Subedi R, et al. *Science* 320:1476 (2008)
46. Hen O, et al. *Science* 346:614 (2014)
47. Duer M, et al. *Phys. Rev. Lett.* 122:172502 (2019)
48. Duer M, et al. *Nature* 560:617 (2018)
49. Cruz-Torres R, et al. *Phys. Lett. B* 797:134890 (2019)
50. Nguyen D, et al. *Phys. Rev. C* 102:064004 (2020)
51. Cruz-Torres R, et al. *Phys. Rev. Lett.* 124:212501 (2020)
52. Li S, et al. The isospin structure of short-range correlations in the mirror nuclei ^{3}H and ^{3}He. *Nature*. In press (2022)
53. Korover I, et al. *Phys. Lett. B* 820:136523 (2021)
54. Schmidt A, et al. *Nature* 578:540 (2020)
55. Weiss R, Bazak B, Barnea N. *Phys. Rev. C* 92:054311 (2015)
56. Weiss R, Cruz-Torres R, Barnea N, Piasetzky E, Hen O. *Phys. Lett. B* 780:211 (2018)
57. Sargsian MM, Abrahamyan TV, Strikman MI, Frankfurt LL. *Phys. Rev. C* 71:044615 (2005)
58. Pybus JR, Korover I, Weiss R, Schmidt A, Barnea N, et al. *Phys. Lett. B* 805:135429 (2020)
59. Patsyuk M, et al. *Nat. Phys.* 17:693 (2021)
60. Hen O, et al. *Studying short-range correlations with real photon beams at GlueX*. Propos. PR12-19-003, Jefferson Lab, Newport News, VA (2019)
61. Higinbotham D, Piasetzky E, Strikman M. *CERN Courier* 49N1:22 (2009)
62. Frankfurt L, Sargsian M, Strikman M. *Int. J. Mod. Phys. A* 23:2991 (2008)
63. Kulagin SA, Petti R. *Phys. Rev. D* 76:094023 (2007)
64. Niewczas K, Sobczyk JT. *Phys. Rev. C* 93:035502 (2016)
65. Van Cuyck T, et al. *Phys. Rev. C* 94:024611 (2016)
66. Ciofi degli Atti C, Mezzetti CB, Morita H. *Phys. Rev. C* 95:044327 (2017)
67. Carlson J, et al. *Rev. Mod. Phys.* 87:1067 (2015)
68. Sobczyk JE, Acharya B, Bacca S, Hagen G. *Phys. Rev. Lett.* 127:072501 (2021)
69. Aubert JJ, et al. *Phys. Lett. B* 123:275 (1983)
70. Gomez J, et al. *Phys. Rev. D* 49:4348 (1994)
71. Sick I, Day D. *Phys. Lett. B* 274:16 (1992)
72. Geesaman DF, Saito K, Thomas AW. *Annu. Rev. Nucl. Part. Sci.* 45:337 (1995)
73. Malace S, Gaskell D, Higinbotham DW, Cloet I. *Int. J. Mod. Phys. E* 23:1430013 (2014)
74. Miller GA, Smith JR. *Phys. Rev. C* 65:015211 (2002). Erratum. *Phys. Rev. C* 66:049903 (2002)
75. Smith JR, Miller GA. *Phys. Rev. C* 65:055206 (2002)
76. Cloët IC, et al. *J. Phys. G* 46:093001 (2019)

77. Seely J, et al. *Phys. Rev. Lett.* 103:202301 (2009)
78. Arrington J, et al. *Phys. Rev. C* 104:065203 (2021)
79. Higinbotham DW, Gomez J, Piasetzky E. arXiv:1003.4497 [hep-ph] (2010)
80. Weinstein LB, et al. *Phys. Rev. Lett.* 106:052301 (2011)
81. Hen O, Piasetzky E, Weinstein LB. *Phys. Rev. C* 85:047301 (2012)
82. Arrington J, Fomin N. *Phys. Rev. Lett.* 123:042501 (2019)
83. Arrington J, et al. *Inclusive scattering from nuclei at x > 1 in the quasielastic and deeply inelastic regimes*. Propos. P12-06-105, Jefferson Lab, Newport News, VA (2006)
84. Arrington J, et al. *Detailed studies of the nuclear dependence of* F_2 *in light nuclei*. Propos. PR12-10-008, Jefferson Lab, Newport News, VA (2010)
85. Arrington J, Coester F, Holt RJ, Lee TSH. *J. Phys. G* 36:025005 (2009)
86. Arrington J, Rubin JG, Melnitchouk W. *Phys. Rev. Lett.* 108:252001 (2012)
87. Accardi A, et al. *Phys. Rev. D* 81:034016 (2010)
88. Accardi A, et al. *Phys. Rev. D* 84:014008 (2011)
89. Abrams D, et al. arXiv:2104.05850 [hep-ex] (2021)
90. Cocuzza C, et al. *Phys. Rev. Lett.* 127:242001 (2021)
91. Segarra EP, et al. arXiv:2104.07130 [hep-ph] (2021)
92. Dutta D, Peng JC, Cloet IC, Gaskell D. *Phys. Rev. C* 83:042201 (2011)
93. Dutta D, et al. *Precise measurement of* π^+/π^- *ratios in semi-inclusive deep inelastic scattering part II: unraveling the flavor dependence of the EMC effect*. Propos. PR12-09-004, Jefferson Lab, Newport News, VA (2009)
94. Weinstein L, et al. *Semi-inclusive deep inelastic scattering measurement of A = 3 nuclei with CLAS12 in Hall B*. Propos. PR12-21-004, Jefferson Lab, Newport News, VA (2021)
95. Cloet IC, Bentz W, Thomas AW. *Phys. Rev. Lett.* 109:182301 (2012)
96. Arrington J, et al. *First measurement of the flavor dependence of nuclear PDF modification using parity violating deep inelastic scattering*. Propos. PR12-21-002, Jefferson Lab, Newport News, VA (2021)
97. Ye Z, et al. *Phys. Rev. C* 97:065204 (2018)
98. Higinbotham DW, Hen O. *Phys. Rev. Lett.* 114:169201 (2015)
99. Freese AJ, Sargsian MM, Strikman MI. *Eur. Phys. J. C* 75:534 (2015)
100. Arrington J, Fomin N, Li S. *3N short range correlations*. Letter of Intent LOI12-21-001, Jefferson Lab, Newport News, VA (2021)
101. Ye Z, Arrington J. arXiv:1810.03667 [nucl-ex] (2018)
102. Hen O, et al. *Exclusive studies of short range correlations in nuclei using CLAS12*. Exp. E12-17-006A, Jefferson Lab, Newport News, VA (2018)
103. Bickerstaff RP, Birse MC, Miller GA. *Phys. Rev. Lett.* 53:2532 (1984)
104. Melnitchouk W, Sargsian M, Strikman MI. *Z. Phys. A* 359:99 (1997)
105. Melnitchouk W, Schreiber AW, Thomas AW. *Phys. Rev. D* 49:1183 (1994)
106. Mulders PJ, Thomas AW. *Phys. Rev. Lett.* 52:1199 (1984)
107. Fomin N, et al. *Phys. Rev. Lett.* 105:212502 (2010)
108. Brodsky SJ, Robertson DG. In *Confinement Physics: Proceedings of the First ELFE Summer School*, ed. SD Bass, PAM Guichon, pp. 71–110. Gif-sur-Yvette, Fr.: Ed. Front. (1996)
109. Brodsky SJ. In *Hadron Physics*, ed. IJD MacGregor, R Kaiser, pp. 121–73. Boca Raton, FL: CRC Press (2006)
110. Brodsky SJ. *Eur. Phys. J. A* 24S1:129 (2005)
111. Ji CR, Brodsky SJ. *Phys. Rev. D* 34:1460 (1986)
112. Souder P, et al. *Precision measurement of parity-violation in deep inelastic scattering over a broad kinematic range*. Exp. E12-10-007, Jefferson Lab, Newport News, VA (2010)
113. Cosyn W, Sargsian M. *Int. J. Mod. Phys. E* 26:1730004 (2017)
114. Strikman M, Weiss C. *Phys. Rev. C* 97:035209 (2018)
115. Baillie N, et al. *Phys. Rev. Lett.* 108:142001 (2012). Erratum. *Phys. Rev. Lett.* 108:199902 (2012)
116. Tkachenko S, et al. *Phys. Rev. C* 89:045206 (2014). Addendum. *Phys. Rev. C* 90:059901 (2014)
117. Griffioen KA, et al. *Phys. Rev. C* 92:015211 (2015)
118. Bueltmann S, et al. *The structure of the free neutron at large x-bjorken*. Propos. P12-06-113, Jefferson Lab, Newport News, VA (2006)

119. Hen O, et al. *In medium proton structure functions, SRC, and the EMC effect*. Exp. E12–11-003A, Jefferson Lab, Newport News, VA (2015)
120. Hen O, Gilad S, Weinstein L, Wood S. *In medium nucleon structure functions, SRC, and the EMC effect*. Exp. E12-11-107, Jefferson Lab, Newport News, VA (2011)
121. Jentsch A, Tu Z, Weiss C. *Phys. Rev. C* 104:065205 (2021)
122. Arrington J, et al. arXiv:2112.00060 [nucl-ex] (2021)

Annual Review of Nuclear and Particle Science

Volume 72, 2022

Contents

Errata

An online log of corrections to *Annual Review of Nuclear and Particle Science* articles may be found at http://www.annualreviews.org/errata/nucl